bioRxiv preprint doi: https://doi.org/10.1101/170381; this version posted July 9, 2019. The copyright holder for this preprint (which was not certified by peer review) is the author/funder, who has granted bioRxiv a license to display the preprint in perpetuity. It is made available under aCC-BY-NC-ND 4.0 International license.

Impact of spatial scale and edge weight on predictive power of cortical thickness networks

Pradeep Reddy Raamana[1], Stephen C. Strother[1,2], and for The Alzheimer's Disease Neuroimaging Initiative

[1]Rotman Research Institute, Baycrest Health Sciences, Toronto, ON, Canada.

[2]Department of Medical Biophysics, University of Toronto, Toronto, ON, Canada.

Abstract

Network-level analysis based on anatomical, pairwise similarities (e.g., cortical thickness) has been gaining increasing attention recently. However, there has not been a systematic study of the impact of spatial scale and edge definitions on predictive performance. In order to obtain a clear understanding of relative performance, there is a need for systematic comparison. In this study, we present a histogram-based approach to construct subject-wise weighted networks that enable a principled comparison across different methods of network analysis. We design several weighted networks based on two large publicly available datasets and perform a robust evaluation of their predictive power under three levels of separability. One of the interesting insights is that changes in nodal size (spatial scale) have no significant impact on predictive power among the three classification experiments and two disease cohorts studied, i.e., mild cognitive impairment and Alzheimer's disease from ADNI, and Autism from the ABIDE dataset. We also release an open source python package to enable others to implement the novel network feature extraction algorithm, which is applicable to other modalities in diverse applications of connectivity research.

Index Terms: cortical thickness, graph theory, early detection, mild cognitive impairment, alzheimer, model comparison, histogram distance, magnetic resonance imaging

Introduction

Alzheimer's disease (AD) is a deadly brain disorder that is expected to result in health-care burden of over $250 billion in 2017 alone (Alzheimer's Association 2017). Although there has been great progress in the last few decades in accurately characterizing AD as well as its progression (Weiner et al. 2017, 2013, 2015), its translation to improvement of clinical trials continues to be a great challenge (Cummings, Morstorf, and Zhong 2014). For any preventive or disease-modifying therapies to succeed, early detection is key, and much of the development of network-level detection techniques has occurred in the AD using the ADNI data sets.

[1] Corresponding author email: praamana@research.baycrest.org

bioRxiv preprint doi: https://doi.org/10.1101/170381; this version posted July 9, 2019. The copyright holder for this preprint (which was not certified by peer review) is the author/funder, who has granted bioRxiv a license to display the preprint in perpetuity. It is made available under aCC-BY-NC-ND 4.0 International license.

Regional and network-level analyses of features derived from multiple modalities such as structural magnetic resonance imaging (sMRI) (Cuingnet et al. 2011; Bron et al. 2015; Duchesne et al. 2008; Dyrba, M., Barkhof, F., Fellgiebel, A., Filippi, M., Hausner, L., Hauenstein, K., Kirste, T. and Teipel, S.J. 2015), positron emission tomography (PET) (Dukart et al. 2011; Herholz et al. 2002; Matthews et al. 2016) and resting-state functional MRI (rs-fMRI) (Hojjati, Ebrahimzadeh, and Khazaee 2017; Abraham et al. 2017) are showing great promise in identifying differences between health and disease in the early stages, as well as establishing how they correlate with cognitive measures (Alexander-Bloch, Giedd, and Bullmore 2013; Tijms et al. 2013). Multimodal predictive modeling methods typically demonstrate high prognostic accuracy (Sui et al. 2011; Arbabshirani et al. 2017) in many applications, owing to their training based on multiple sets of rich and complementary information related to disease. However, recent efforts in building more sophisticated machine learning strategies produced unimodal sMRI methods rivaling the state-of-the-art multimodal approaches (Weiner et al. 2017). Although multi-modal approaches tend to be more sensitive in general and offer richer insight, the practical advantages of sMRI being non-invasive, cost-effective and widely-accessible in the clinic, make sMRI-based computer-aided diagnostic methods for early detection highly desirable.

Cortical thickness is a sensitive imaging biomarker that can be easily derived from sMRI to diagnose AD. However, its sensitivity to identify the prodromal subjects (such as mild cognitive impairment (MCI)) at risk of progressing to AD is limited (Cuingnet et al. 2011). Network-level analysis of cortical thickness and gray matter features demonstrated its potential to provide novel insights or improve predictive power (Raamana et al. 2015), and is gaining in popularity (Evans 2013; Wen, He, and Sachdev 2011; Reid and Evans 2013; Jason P. Lerch et al. 2006). Thickness network features offer complementary information compared to the underlying fiber density (Gong et al. 2012) and have been shown to have potential for early detection of AD (Raamana et al. 2015; Wee et al. 2012; Dai et al. 2012; Kim et al. 2016), as well as for subtype discrimination (Raamana, Wen, et al. 2014), outperforming the non-network raw-thickness features.

Network analysis studies in cortical thickness range from

1. group-wise studies building networks based on group-wise covariance/correlation in cortical thickness (Evans 2013; He and Chen 2007; Jason P. Lerch et al. 2006), which may be used to characterize the properties of these networks (such as small-worldness) as well as provide useful insight into network-level changes between two diagnostic groups e.g. healthy controls (CN) and Alzheimer's disease (AD),
2. studies building individual subject-wise graphs based on within-subject ROI-wise (pairwise) similarity metrics (Raamana et al. 2015; Tijms et al. 2012; Wee et al. 2012; Dai et al. 2012; Kim et al. 2016) to enable predictive modeling. These studies resulted in disease-related insights into network-level imaging biomarkers and improved accuracy for the early detection of AD. However, these studies are based on distinctly different parcellation schemes of the cortex, vastly different ways of linking two different regions in the brain, and datasets differing in size and demographics.

Insights derived from various brain network studies showed considerable variability in reported group differences (Tijms et al. 2013), and widely accepted standards for network construction are yet to be established (Stam 2014). There have been recent efforts into understanding the importance and impact of graph creation methods, sample sizes and density (van Wijk, Stam, and Daffertshofer 2010; Phillips et al. 2015) and their anatomical plausibility (Seidlitz et al. 2017). However, these studies have been restricted to the choice of group-wise correlation methods to define the edges, or limited to understanding the group-wise differences in selected graph measures. But such important methodological analyses have not been performed in the context of building individual subject-wise predictive modelling. Hence, there is no clear understanding of the impact of different choices in subject-wise network construction and their relative predictive performance.

bioRxiv preprint doi: https://doi.org/10.1101/170381; this version posted July 9, 2019. The copyright holder for this preprint (which was not certified by peer review) is the author/funder, who has granted bioRxiv a license to display the preprint in perpetuity. It is made available under aCC-BY-NC-ND 4.0 International license.

Given their potential for the development of accurate early detection methods (Raamana et al. 2015; Raamana, Wen, et al. 2014) demonstrated by outperforming non-network raw-thickness features, and the wide-accessibility of sMRI, thickness-based networks deserve a systematic study in terms of

1. how does the choice of edge weight or linking criterion (correlation (He and Chen 2007), similarity (Raamana et al. 2015) affect the performance of the predictive models? See Table 3 for more details.
2. how does the scale of parcellation (size and number of cortical ROIs) affect the predictive performance?

These questions, analyzed in our systematic study, can reveal important tradeoffs of this emerging theme of research. In this study, we present a comparison of six different ways of constructing thickness-based, subject-wise networks and present classification results under varyinglevels of separability i.e. in discriminating AD from CN and mild cognitive impairment (MCI) from CN in the ADNI dataset. In order to test whether these results generalize to new datasets, diseases and separability, we also perform the study in discriminating Autism (AUT) subjects from CN in the Autism Brain Imaging Data Exchange (ABIDE) dataset. Based on two large publicly available datasets, we not only to replicate the results on an independent dataset, but also replicate analysis in the presence of a different disease and in a different age group.

Methods

In this section, we describe the datasets we study in detail, along with a detailed description of the preprocessing and the associated methods.

ADNI dataset

Data used in the preparation of this article were obtained from the Alzheimer's Disease Neuroimaging Initiative (ADNI) database (adni.loni.usc.edu). The ADNI was launched in 2003 as a public-private partnership, led by Principal Investigator Michael W. Weiner, MD. The primary goal of ADNI has been to test whether serial magnetic resonance imaging (MRI), positron emission tomography (PET), other biological markers, and clinical and neuropsychological assessment can be combined to measure the progression of mild cognitive impairment (MCI) and early Alzheimer's disease (AD). For up-to-date information, see www.adni-info.org .

We downloaded baseline T1 MRI scans (n=671) from the ADNI dataset (Jack et al. 2008), which has quality-controlled Freesurfer parcellation (version 4.3) of the cortical surfaces provided in the ADNI portal (B. Fischl and Dale 2000; Bruce Fischl et al. 2002). The parcellation and cortical thickness values downloaded were carefully visually inspected for errors in geometry and range. When noticeable errors were found, we eliminated those (n=24) subjects, and no manual editing and corrections were performed. The thickness features from the remaining subjects for the control (CN) and AD groups (effective n=647) comprised the first set of subjects for our analysis in this study. The second set of subjects with a slightly lower level of separability (MCI subjects converting to AD in 18 months, denoted by MCIc) were chosen to match the benchmarking study (Cuingnet et al. 2011) as closely as possible (to enable comparison to the many methods included) based on data availability and quality control results. The demographics for the two sets are listed in Table 1.

bioRxiv preprint doi: https://doi.org/10.1101/170381; this version posted July 9, 2019. The copyright holder for this preprint (which was not certified by peer review) is the author/funder, who has granted bioRxiv a license to display the preprint in perpetuity. It is made available under aCC-BY-NC-ND 4.0 International license.

TABLE 1: *ADNI I Demographics*

Diagnostic Group	N	Females	Age	MMSE*
Dataset 1: ADNI				
Healthy controls (CN1)	224	109	75.79 (4.99)	29.11 (1.01)
Alzheimer's disease (AD)	188	89	75.22 (7.49)	23.29 (2.04)
Dataset 2: ADNI				
Healthy controls (CN2, for MCI)^	159	85	76.07 (5.33)	29.17 (0.98)
MCI converters to AD in 18 months (MCIc)	76	33	74.67 (7.35)	26.47 (1.86)

All statistics here are displayed in mean (SD) format.
*ADNI: Only MMSE is significantly different between CN1 & AD with $p < 0.05$.
^ADNI: Controls and MCI converters are chosen to match the benchmark samples presented in (Cuingnet et al. 2011) as closely as possible allowing for exclusions due to quality control.

ABIDE dataset

In order to study whether the conclusions drawn from the ADNI dataset generalize to a different dataset and a different disease cohort, we obtained the Freesurfer parcellations (version 5.1) from the the Autism Brain Imaging Data Exchange (ABIDE) preprocessed dataset made available freely on the ABIDE website (Craddock, Cameron and Benhajali, Yassine and Chu, Carlton and Chouinard, Francois and Evans, Alan and Jakab, Andr?s and Khundrakpam, Budhachandra Singh and Lewis, John David and Li, Qingyang and Milham, Michael and Yan, Chaogan and Bellec, Pierre 2013). A random subset of cortical parcellations (n=227) have been visually inspected for errors in geometry estimation and value ranges to eliminate any subjects showing even a mild chance of failure. From the passing subjects (n=226), we randomly selected 200 subjects (100 samples per diagnostic group) whose demographics are presented in Table 2 and the subject IDs are listed in the Appendix. Owing to the random selection, they come from multiple sites, which is akin to the ADNI dataset used in this study. Previous research (Abraham et al. 2017) showed that the site heterogeneity has little or no impact on the predictive accuracy of network-level features derived from task-free fMRI data. The distribution of the sites represented in this study are shown in Appendix D.

Table 2: *ABIDE I demographics*

Dataset 3: ABIDE						
Diagnostic Group	N	Females	Age	FIQ*	PIQ	VIQ*
Healthy controls (CN3)	100	17	17.27 (7.68)	109.10 (12.35)	105.64 (12.74)	111.89 (13.52)
Autism (AUT)	100	9	15.82 (5.93)	103.49 (14.68)	104.57 (14.68)	101.36 (15.86)
ABIDE: FIQ and VIQ are significantly different between CN3 & AUT with $p < 0:05$. FIQ: Full IQ standard score VIQ: Verbal IQ standard score PIQ: Performance IQ standard score						

bioRxiv preprint doi: https://doi.org/10.1101/170381; this version posted July 9, 2019. The copyright holder for this preprint (which was not certified by peer review) is the author/funder, who has granted bioRxiv a license to display the preprint in perpetuity. It is made available under aCC-BY-NC-ND 4.0 International license.

Feature extraction

In the following sections, we describe the steps involved in the extraction of weighted networks based on T1 MRI scans of the different subjects in the two independent datasets.

Alignment and dimensionality reduction

Cortical thickness features studied here were obtained from the Freesurfer parcellations. They were then resampled to the *fsaverage* atlas and smoothed at *fwhm*=10mm. This is achieved by Freesurfer `-qcache` processing option, which registers each of the subjects to the *fsaverage* atlas (provided with Freesurfer) to establish vertex-wise correspondence across all the subjects.

Cortical subdivision

In order to avoid the curse of dimensionality and to reduce the computational burden, the atlas has been subdivided using a surface-based, patch-wise parcellation technique originally presented in (Raamana et al. 2015). Here, we use an adaptive version wherein the patch-size is controlled by number of vertices (denoted by *m*=vertices/patch), instead of choosing a globally fixed number of patches (say 10) per Freesurfer APARC label regardless of its size (which can vary widely resulting in vastly different patch sizes within the same subject). As we change *m*, the subdivision of the cortical labels is performed purely on the existing mesh, and neither the geometrical parcellation itself nor the vertex density are modified. Here, *m* can be taken as the size of the graph node (imagine the node as a small patch within different Freesurfer labels). Alternatively, *m* can be seen as the spatial scale of the graph analysis, whose impact is being assessed for different values of *m*. When m is small (say 100), this results in large number (273) of total patches (sum of number of patches for each aparc label) across the whole cortex, whereas it results in only 68 patches when it is very high (m=10000), as such a large patch covered the full extent of all the 68 Freesurfer APARC labels currently defined on fsaverage cortical parcellation. We have analyzed the following values of *m*= 1000, 2000, 3000, 5000 and 10000, which resulted in the following total number of non-overlapping patches in the whole cortex: 273, 136, 97, 74 and 68 respectively.

Table 3

Type of base representation	Type of edge weight metric	Acronym	Mathematical definition
Summarized (median/mean in a patch)	Similarity (Raamana et al. 2015)	MD	$\lvert M_i - M_j \rvert$
	exp(similarity)	EMD	$e^{-\frac{(\mu_i-\mu_j)^2}{2(\sigma_i+\sigma_j)}}$
Raw distribution	Wilcoxon ranksum statistic	RS	Ranksum test statistic
Normalized histogram	Histogram correlation	HCOR	$\rho(h_i, h_j)$
	X^2 statistic	CHI2	$2\sum_{k=1}^{N} \frac{(h_i(k) - h_j(k))^2}{h_i(k) + h_j(k)}$

bioRxiv preprint doi: https://doi.org/10.1101/170381; this version posted July 9, 2019. The copyright holder for this preprint (which was not certified by peer review) is the author/funder, who has granted bioRxiv a license to display the preprint in perpetuity. It is made available under aCC-BY-NC-ND 4.0 International license.

	Histogram intersection	HINT	$\frac{\sum_{k=1}^{N} min(h_i(k), h_j(k))}{\sum_{k=1}^{N} h_i(k)}$

For patches i and j, M, μ and σ are the median, mean and standard deviation of a patch-wise distribution of vertex-wise thickness values, h_i is the normalized histogram of a given distribution. N is the number of bins in histogram, which is fixed at N=100 bins. Here, ρ is the Pearson correlation coefficient between two vectors of equal length.

Network Computation

Construction of thickness networks in their early form were based on group-wise correlations (He and Chen 2007). Our previous publications based on cortical thickness (Raamana et al. 2015; Raamana, Wen, et al. 2014) and other interesting studies on gray matter density (Tijms et al. 2012; Wee et al. 2012) extend the earlier approaches to individualized subject-wise network extraction methods. Many of these previous studies relied on summarizing the thickness distribution in a given ROI (e.g. using mean within the entire Freesurfer label as in (Tijms et al. 2012)) or within a patch (Freesurfer label subdivided further as in (Raamana et al. 2015)), before constructing the networks. Although such approaches reduce the dimensionality and provide us with smooth features, they do not utilize the rich description and variance of the distribution of features. Moreover, studies thus far computed characteristic features from a binary network (by applying an optimized threshold (Raamana et al. 2015)) or using a vector representation of weighted graphs (vector of distances in the upper triangular part of the edge weight matrix, as they are symmetric (Tijms et al. 2012)). Here, in order to enable a principled comparison across the different edge weights (and to avoid the optimization of an arbitrary threshold required to binarize the edge weight matrix), we study weighted-networks only, whose derivation is described below.

Histogram WEighted NETworks (HiWeNet)

In this section, we describe the method employed in constructing the Histogram WEighted NEtworks (HiWeNet) based on cortical thickness. First, to improve the robustness of the features, 5% outliers from both tails of the distribution of cortical thickness values are discarded from each patch at a given scale *m* (see Appendix for more information). The residual distribution is converted into a histogram by binning into uniformly spaced $n = 100$ bins. Then the histogram counts are normalized using

$$\mathrm{h}_i(k) = \frac{h_i(k)}{\sum_{k=1}^{N} h_i(k)}$$

for $k = 1 : N$, where h_i is the histogram of patch *i*. This method (illustrated further in Figure 1) enables the computation of the pairwise edge-weight (distance between the histograms, denoted by EW) for the two patches *i* and *j*. A variety of histogram distances as listed in Table 3 are studied in this paper to analyze their impact on predictive power.

bioRxiv preprint doi: https://doi.org/10.1101/170381; this version posted July 9, 2019. The copyright holder for this preprint (which was not certified by peer review) is the author/funder, who has granted bioRxiv a license to display the preprint in perpetuity. It is made available under aCC-BY-NC-ND 4.0 International license.

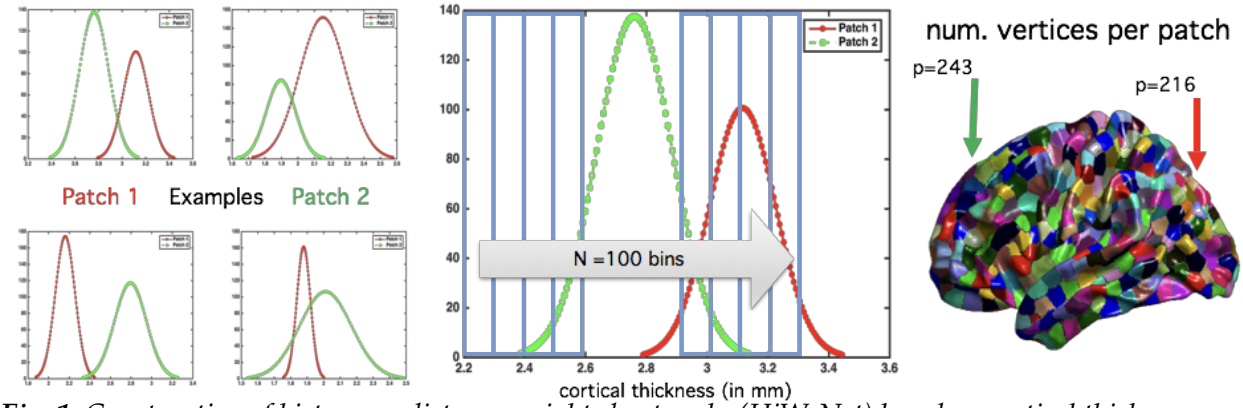

***Fig. 1**: Construction of histogram-distance weighted networks (HiWeNet) based on cortical thickness features using edge-weight calculations (applicable to HCOR, CHI2 and HINT metrics in Table 3). The four smaller subpanels on the left show typical distributions of cortical thickness values for four random pairs of patches (in green and red) in a given subject (shown on cortical visualization on right). They demonstrate the means and shape of these distributions can vary substantially as you traverse across different pairs of cortical patches. The large panel in the middle illustrates the type of binning used to construct the histogram from each patch.*

To analyze the relative benefit of HiWeNet, we compare the histogram-based methods to three commonly used inter-nodal weights based on descriptive summary statistics (denoted as MD, EMD and RS in Table 3). Once the edge weight matrix is computed (which is symmetric), we extract the upper-triangular part of the matrix and vectorize it (of length $n*(n-1)/2$, where n is the number of patches on the cortex for a given number of vertices/patch m). The vectorized array of edge weights (VEW) forms the input to the classifier. Each element of VEW corresponds to a unique edge in the matrix of pairwise edges. In addition, in Appendix C, we present and analyze the performance of an alternative network-representation method.

Note on test-retest reliability

The reliability of this network approach developed in *HiWeNet* (pairwise distances between ROIs) boils down to the reliability of the method to measure cortical thickness at the vertex-level, as the remaining parts of algorithm are deterministic. Several studies have previously shown that cortical thickness estimation (and Freesurfer as a tool) have high test-retest reliability (Han et al. 2006; Iscan et al. 2015) and it has no impact on brain-behaviour relationships (Dickerson et al. 2008). In addition, given our choice of employing distance between thickness distributions over relatively large patches (1000 vertices or more), small changes in thickness (e.g. 0.2mm) would be absorbed into the distance calculations, and hence are unlikely to change the results presented herein.

Open source software

Almost all of the computational code related to this study had been implemented in Matlab. In order to enable other researchers to utilize the presented feature extraction technique, we have re-implemented the core HiWeNet algorithm in Python and made it publicly available at this URL: https://github.com/raamana/hiwenet (Raamana and Strother 2017). Note this python package has not been used to produce the current results, but has been re-implemented by Raamana in Python to contribute to open source and also to make it accessible to broader audience who may not have access to expensive Matlab licenses. We have also published the original matlab code for the computation of adjacency matrices used for this study, within the the *hiwenet* python package.

bioRxiv preprint doi: https://doi.org/10.1101/170381; this version posted July 9, 2019. The copyright holder for this preprint (which was not certified by peer review) is the author/funder, who has granted bioRxiv a license to display the preprint in perpetuity. It is made available under aCC-BY-NC-ND 4.0 International license.

Further, in order to make this research even more accessible, we have implemented the entire workflow of morphometric network extraction as a seamless pipeline called graynet, implemented entirely in Python (Raamana and Strother 2018). Using this tool would enable those without much software engineering experience to simply run Freesurfer and then run graynet to get started with morphometric network analyses. This frees them from the programming hassle of assembling complicated data and extracting graph theoretical operations, which can be a barrier to many laboratories.

Comparison of predictive utility

In this section, we describe the procedure and techniques used to evaluate and compare the predictive power of multiple variations of the network-level features. Thanks to the relatively large sample sizes, we could employ a repeated nested split-half cross-validation (CV) scheme, with 50% reserved for training, in order to maximize the sizes of training and test sets. Moreover, in each iteration of CV, all the methods are trained and assessed on the exact same training and test sets, in order to "pair" the performance estimates. This technique is shown to produce reliable and stable estimates of differences in predictive performance across different methods (Dietterich 1998; Burman 1989; Demšar 2006), instead of pooling multiple sets of performance distributions estimated separately on different training and test sets for each method independently. This setup allows us to compare large numbers of methods and their variants simultaneously.

Cross-validation scheme

The comparison scheme employed is comprised of the following steps:

1) repeated split-half cross-validation scheme, with class-sizes stratified in the training set (RHsT) (Raamana et al. 2015), to minimize class-imbalance. This scheme is repeated N=200 times, to obtain the N paired estimates of classification performance.
2) In each CV run,
    a) feature selection (from VEW) on one split (training set of size N_{train}) is performed based on t-statistic based ranking (based on group-wise differences in the training set only), selecting only the top $N_{train}/10$ elements. The frequency of selection of a particular element (which is an edge in the cortical space) over different CV trials by the t-statistic ranking is an indication of its discriminative utility, and will be visualized to obtain better insight into the process.
    b) Support vector machine (SVM) is chosen as the classifier to discriminate the two groups in each experiment. SVM is optimized in an inner split-half CV applied to the training set via a grid search. We have employed the following ranges of values in the grid search for the margin control parameter $C = 10^p$; $p = 3 : 5$ and the kernel bandwidth $= 2^q$; $q = 5 : 4$.
    c) The optimized SVM is tested on the second split (test) to evaluate its performance.
3) The process in Step 2 is repeated N=200 times (Varoquaux et al. 2016; Raamana et al. 2015) to obtain 200 independent estimates for each method being compared.
4) In this study, we measure the performance by area under the predictive receiver operating characteristic (ROC) curve (denoted by AUC), whose distributions for different methods are shown in Figure 3.

The results in study were produced using Raamana's programming library implemented in Matlab based on the builtin statistics and machine learning toolbox.

Open source tool to evaluate predictive utility: In order to enable much wider audience (those without access to a Matlab license, or those who do not have the necessary programming skills), we have also built an open source tool called *neuropredict* (Raamana 2017). Once the researchers

bioRxiv preprint doi: https://doi.org/10.1101/170381; this version posted July 9, 2019. The copyright holder for this preprint (which was not certified by peer review) is the author/funder, who has granted bioRxiv a license to display the preprint in perpetuity. It is made available under aCC-BY-NC-ND 4.0 International license.

run Freesurfer successfully, they can run *graynet* (Raamana and Strother 2018), which produces the necessary single-subject morphometric networks. The outputs from graynet in turn serve as direct input to neuropredict, which runs the cross-validation scheme described in the above section to produce a comprehensive report on their predictive power.

Results and Discussion

Within-group networks

To obtain better insight into the topology of the networks defined above, it is helpful to visualize seed-based networks and analyze their connections. A common approach to this end involves picking the posterior cingulate gyrus (core hub of the default mode network, DMN) as the seed and analyzing its connections in healthy controls, and esp. how they change for different edge metrics. The seed-based network visualizations are produced for each edge weight method separately for m=2000, identical to the network construction method described in the Methods section: compute histogram-distance between the thickness distribution of the seed and all the other ROIs, averaging this edge weight across all the healthy subjects, and retaining only the strongest edges (top 5%).

To make the comparison across the three datasets easy, they are grouped for each metric e.g. for median difference (MD), the comparison is shown below for healthy controls. From this figure, we can clearly see a pattern resembling the default mode network, in healthy controls from all the three samples. This is consistent with the results reported in previous structural covariance studies (Spreng and Turner 2013; Evans 2013; Spreng et al. 2013; Power et al. 2011).

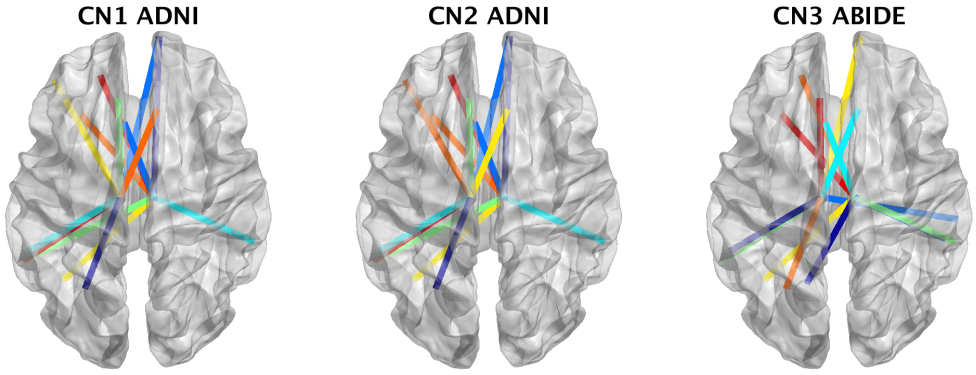

Caption: seed-based connectivity networks for the MD metric (m=2000), showing average weights across each healthy control sample from the three datasets (as labelled). The colors on the edges represent the edge weight using a jet colormap (with blues indicating the weaker and reds indicating stronger weights). From this figure, we can clearly see a pattern resembling the default mode network, in healthy controls from all the three samples.

To get a sense of how these networks change with different EW metric, we show two other networks corresponding to HCOR and CHI2 metrics below (each figure is labelled with the metric and summary statistic being displayed e.g. HCOR mean). This HCOR network loses resemblance to the DMN (e.g. loss of edges to superior frontal, banks of the superior temporal sulcus, frontal pole, fusiform), and the edge weight distribution varies widely across the three samples. However, the CHI2 network resembles the DMN pattern seen in MD network well, suggesting the similarity of the two networks.

bioRxiv preprint doi: https://doi.org/10.1101/170381; this version posted July 9, 2019. The copyright holder for this preprint (which was not certified by peer review) is the author/funder, who has granted bioRxiv a license to display the preprint in perpetuity. It is made available under aCC-BY-NC-ND 4.0 International license.

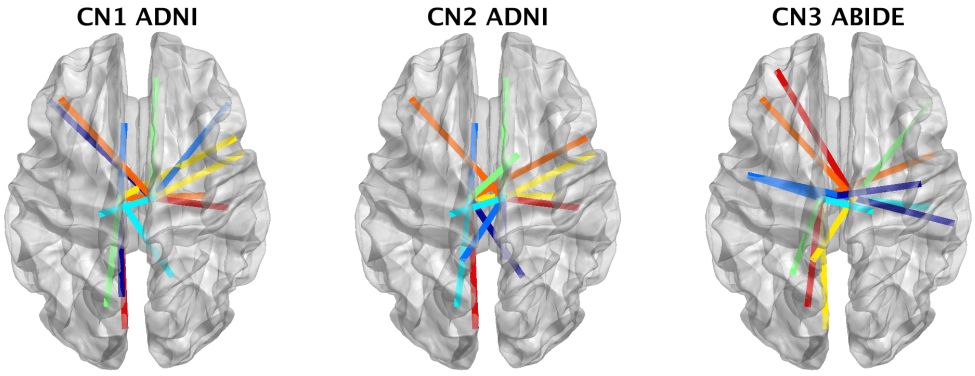

Caption: network showing edge weights(mean across samples) derived via HCOR metric. Layout of the figure is the same as above for the MD network.

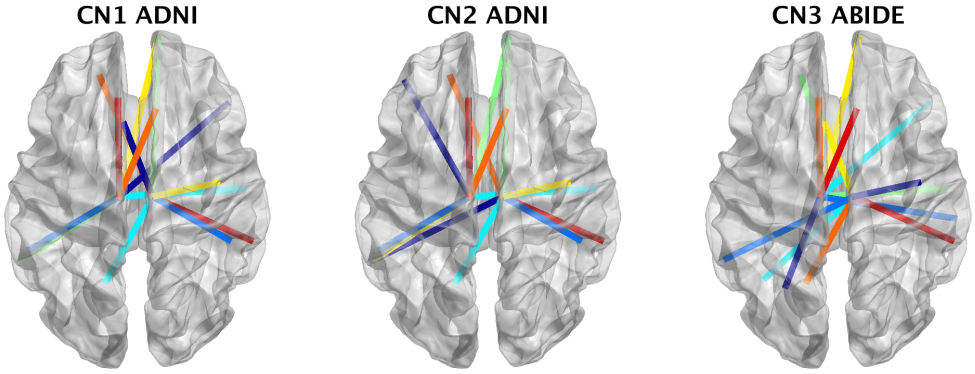

Caption: network showing edge weights (mean across samples) derived via CHI2 metric. Layout of the figure is the same as above for MD.

Group-wise differences

To illustrate the differences between the proposed methods of computing edge weights, we compute the distributions of vertex-wise mean thickness values for CN1 and AD separately. We then visualize them in the form of a matrix of pairwise edge weights at m=2000, as shown in Figures 2 (a) and 2(b). Each row (say node *i)* in a given edge-weight matrix (from one group say CN1 in Fig. 2 (a)) here refers to the pairwise edge weights w.r.t remaining nodes j, $j = 1$:N. As the differences are subtle and spatially distributed, for easy comparison between the two classes, we visualize the arithmetic differences between the two classes in Fig. 2 (c).

The visualizations in Fig. 2(c) offer useful insight into the group-wise differences between CN1 and AD, and across different edge weight distances. However, visual differences do not imply differences in predictive power of features extracted these networks of weights. Hence, it is important to assess their predictive utility in discriminating AD from CN1.

bioRxiv preprint doi: https://doi.org/10.1101/170381; this version posted July 9, 2019. The copyright holder for this preprint (which was not certified by peer review) is the author/funder, who has granted bioRxiv a license to display the preprint in perpetuity. It is made available under aCC-BY-NC-ND 4.0 International license.

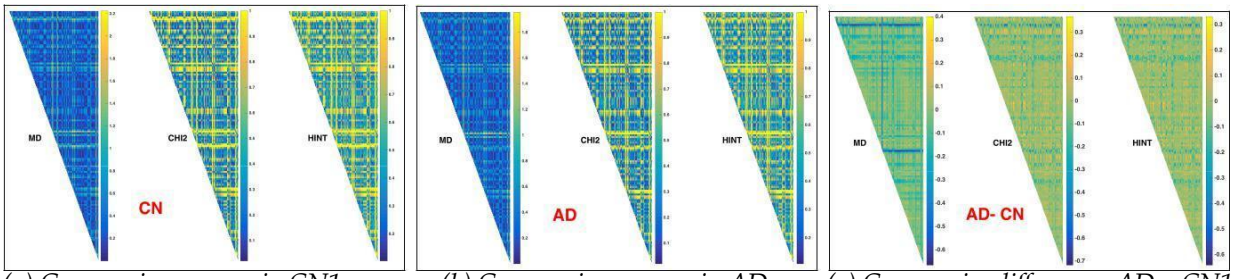

(a) Group-wise average in CN1 *(b) Group-wise average in AD* *(c) Group-wise differences AD – CN1*

***Fig. 2**. Edge weights derived from group-wise average thicknesses for three definitions of edge weight. (a) healthy controls (CN1) (b) Edge weights group-wise average in Alzheimer's disease (AD), both at m=2000. (c) Arithmetic differences i.e. AD – CN1. The three panels in each subfigure show the edge weights from MD, CHI2 and HINT methods as defined in Table 3. In each of the panels, we present the upper triangular part of the edge-weight matrix (pairwise) computed using the corresponding equations in Table 3. We notice there are clear differences among the patterns in the three panels. The panels a and b appear similar at the first glance, but they are sufficiently different to be observed in Fig. 2(c).*

Predictive utility

The RHsT cross-validation scheme is employed for each of the three classification experiments from two independent datasets i.e. CN1 vs. AD, CN2 vs. MCIc and CN3 vs. AUT. The performance distributions for the different combinations are shown in Fig. 3.

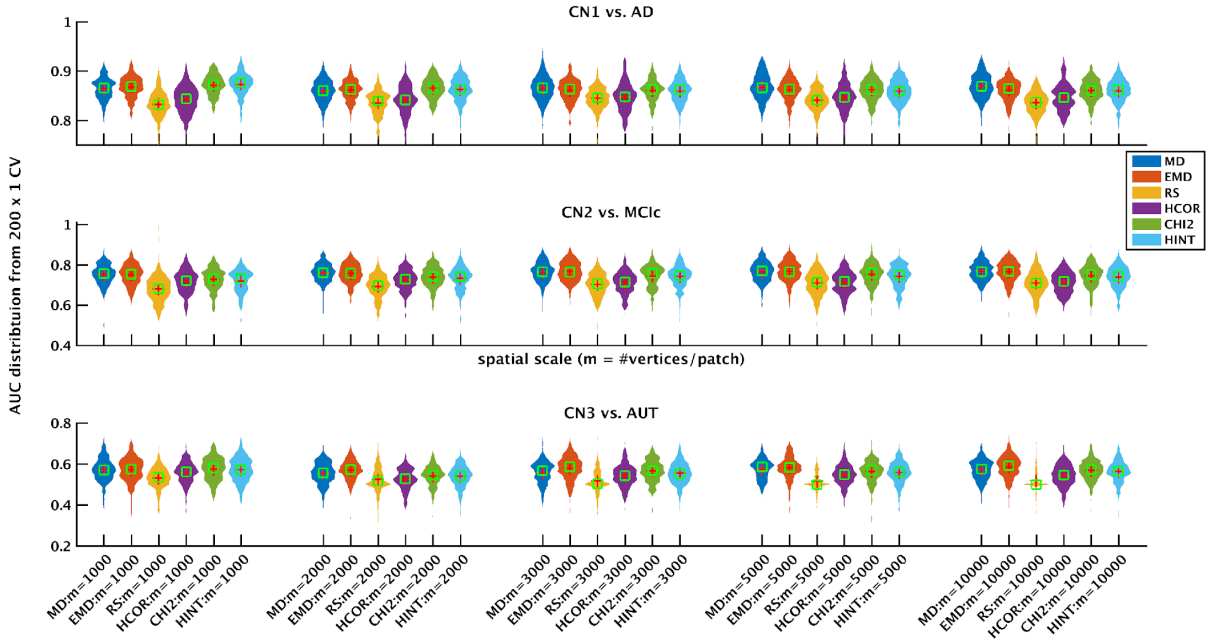

***Fig. 3**. Classification performance for the different network methods (different edge weight metrics at different spatial resolutions of m) in discriminating AD (top panel), MCIc (middle panel) and AUT (bottom) panel from their respective control groups under a rigorous CV scheme. The performance presented here is a distribution of AUC values from 200 randomized train/test splits of RHsT (whose median is shown with a red cross-hair symbol).*

Focusing on the top panel (CN1 vs. AD), there are numerical differences in performance among different methods at fixed scale (m). However, the pattern remains similar across different spatial scales. The MD, EMD, CHI2 and HINT methods are consistently outperforming,

bioRxiv preprint doi: https://doi.org/10.1101/170381; this version posted July 9, 2019. The copyright holder for this preprint (which was not certified by peer review) is the author/funder, who has granted bioRxiv a license to display the preprint in perpetuity. It is made available under aCC-BY-NC-ND 4.0 International license.

numerically speaking, the RS and HCOR methods across different values of *m*. Broadly speaking, the patterns of change in AUC in Fig. 3 within each panel as we move from left to right (going over different combinations) are quite similar to the rest, although at a different median baseline (at AUC=0.87 for CN1 vs. AD, at AUC=0.75 for CN2 vs. MCIc and at AUC=0.6 for CN3 vs. AUT).

Statistical significance testing

In order to assess the statistical significance of differences among this large set of methods, we performed a nonparametric Friedman test (Dietterich 1998) comparing the performance of the 30 different classifiers (6 methods at 5 spatial scales) simultaneously, for each of the three experiments separately. The results from post-hoc Nemenyi test (Demšar 2006) are visualized in a convenient critical difference (CD) diagram (Kourentzes 2016) as shown in Figure 4.

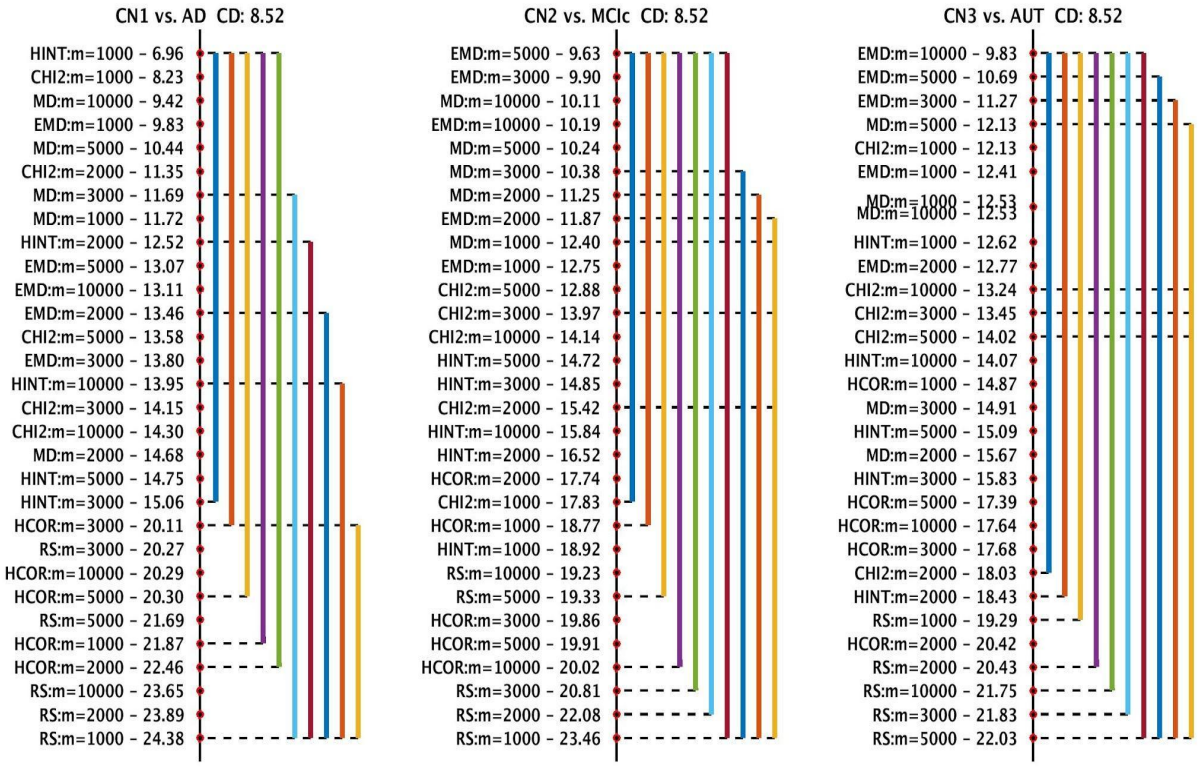

Fig. 4*. Critical difference diagram comparing the ranks of different classification methods in a non-parametric Friedman test based on classification performance results from a rigorous CV evaluation method using 200 iterations of holdout. Here, smaller numerical values for rank implies higher performance. The vertical axis presents the ranks (better ranks and methods at the top, and worse ranks and methods to the bottom). The performance of any two methods are statistically significantly different from each other, if their ranks differ by at least the critical difference (CD), which is noted on top of each of the three panels. If the ranks of a group of methods (annotations on the left within each panel) are connected by a line, they are not statistically significantly different from each other. Different colored lines here present groups of methods that are not significantly different from each other in ranks, each one using a different method as its reference point. For example, in the leftmost panel presenting the results from CN1 vs. AD experiment, the leftmost blue line connects all the methods between the highest ranked HINT:m=1000 (ranked 6.96) to the HINT:m=3000 method (ranked 15.06), including themselves, which implies they are not statistically significantly different from each other. In the same panel, the highest-ranked HINT:m=1000 method is not connected to RS:m=1000 (least-ranked 24.38) via any of the colored lines - hence they are indeed statistically significantly different from each other (difference in ranks higher than CD).*

bioRxiv preprint doi: https://doi.org/10.1101/170381; this version posted July 9, 2019. The copyright holder for this preprint (which was not certified by peer review) is the author/funder, who has granted bioRxiv a license to display the preprint in perpetuity. It is made available under aCC-BY-NC-ND 4.0 International license.

The left panel in Fig. 4 shows that only the top 6 methods (with median ranks from 6.96 to 11.35) are statistically significantly different from the lowest-ranked methods, at α=0.05, correcting for multiple comparisons. The remaining 30 methods, when compared together simultaneously, are not significantly different from each other. The top-ranked 6 methods are not statistically significantly different from each other. We observe a similar pattern in the center panel (CN2 vs. MCIc), except only the top 5 are statistically significantly different from the lowest ranked methods. In the CN3 vs. AUT case, there are no significant differences at all, possibly due to rather low performance from all the methods to begin with (median AUC across methods is around 0.55).

When the comparison is made at a fixed scale m, within each experiment, the performance of the 6 different methods (simultaneous comparison of 6 methods) for most values of m are not statistically significantly different from each other, except for m=1000 (CD diagrams are not shown). When the comparison is done for a fixed edge-weight metric at different values of m, the performance is not statistically significantly different for any m. Also, the top 2 methods are MD and EMD networks (based on differences in median and mean respectively) at the highest resolution m = 1000 and also at the lowest resolution m = 10,000. This indicates that impact of the nodal size on the predictive performance of a network method may be insignificant. This result is consistent with the findings of (Zalesky et al. 2010; Evans 2013), wherein it was observed that group-wise small-worldness and scale-freeness are unaffected by spatial scale.

Most discriminative regions

As noted in our CV section earlier, our method records the frequency (across the N CV iterations) of selection (of each weighted connection in VEW) from the t-statistic based ranking method applied on the training set. This helps us gain insight into which pair-wise links have been most frequently discriminative. This pair-wise link frequency can be mapped back to individual cortical patches for intuitive visualization, identifying most discriminative regions (MDRs). One such visualization, thresholding the importance at 50% derived at m=2000, is shown in Fig 5. Each color on the cortex represents a particular EW metric (labelled on the colorbar) that led to its selection, and when multiple methods selected the same region (indicating additional importance), we painted it red and labelled it "Multiple". Note the input to the SVM classifier was a vector of edge weights (from upper-triangular part of the edge weight matrix), and hence the selection of a particular edge leads to highlighting both the regions forming the link. Moreover, the importance of a particular node (cortical patch) could be accumulated from its multiple links, if any.

Fig. 5 shows the red MDRs (identified by multiple methods as MDR) cover a large cortical area, which is not unexpected, given the changes caused by full AD are known to be widespread over the cortex. In Fig. 6, we observe the MDRs in areas consistently identified with progressive MCI or early stage AD such as middle temporal lobe, cingulate (anterior and inferior), cuneus and precuneus. Of interest here is the clear hemispheric asymmetry to the left, which can also be observed to a lesser extent in the MDRs for AD in Fig. 5. The MDRs identified in discriminating AUT from CN3 are shown in Fig. 7. They appear in the lingual, supra-marginal, post- and precentral areas, which are consistent with previous reports on Autism studying the group differences in developmental patterns of cortical thickness (Smith et al. 2016; Scheel et al. 2011), as well as found to be important in other prediction tasks (Moradi et al. 2017).

bioRxiv preprint doi: https://doi.org/10.1101/170381; this version posted July 9, 2019. The copyright holder for this preprint (which was not certified by peer review) is the author/funder, who has granted bioRxiv a license to display the preprint in perpetuity. It is made available under aCC-BY-NC-ND 4.0 International license.

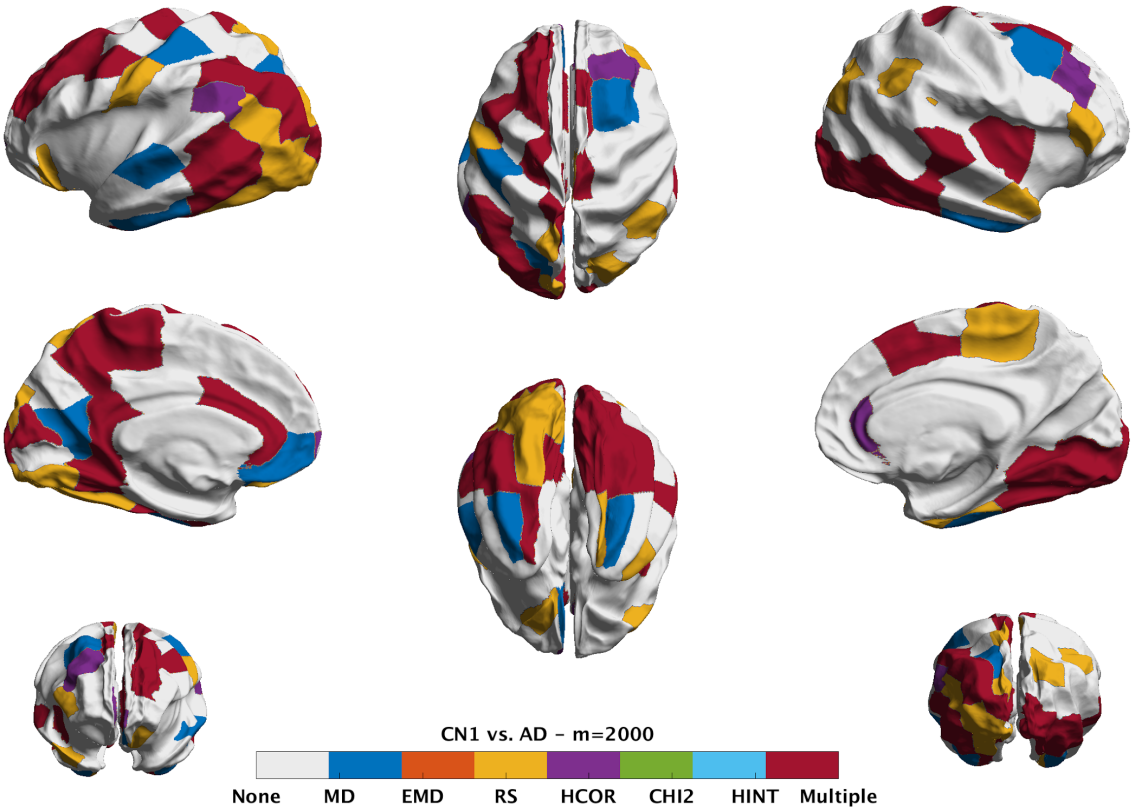

***Fig 5**: Visualization of the most discriminative regions as derived from the CN1 vs. AD experiment at m=2000. Due to distributed nature of the degeneration caused by AD, we expect the MDRs to span a wide area of the cortex as observed here.*

bioRxiv preprint doi: https://doi.org/10.1101/170381; this version posted July 9, 2019. The copyright holder for this preprint (which was not certified by peer review) is the author/funder, who has granted bioRxiv a license to display the preprint in perpetuity. It is made available under aCC-BY-NC-ND 4.0 International license.

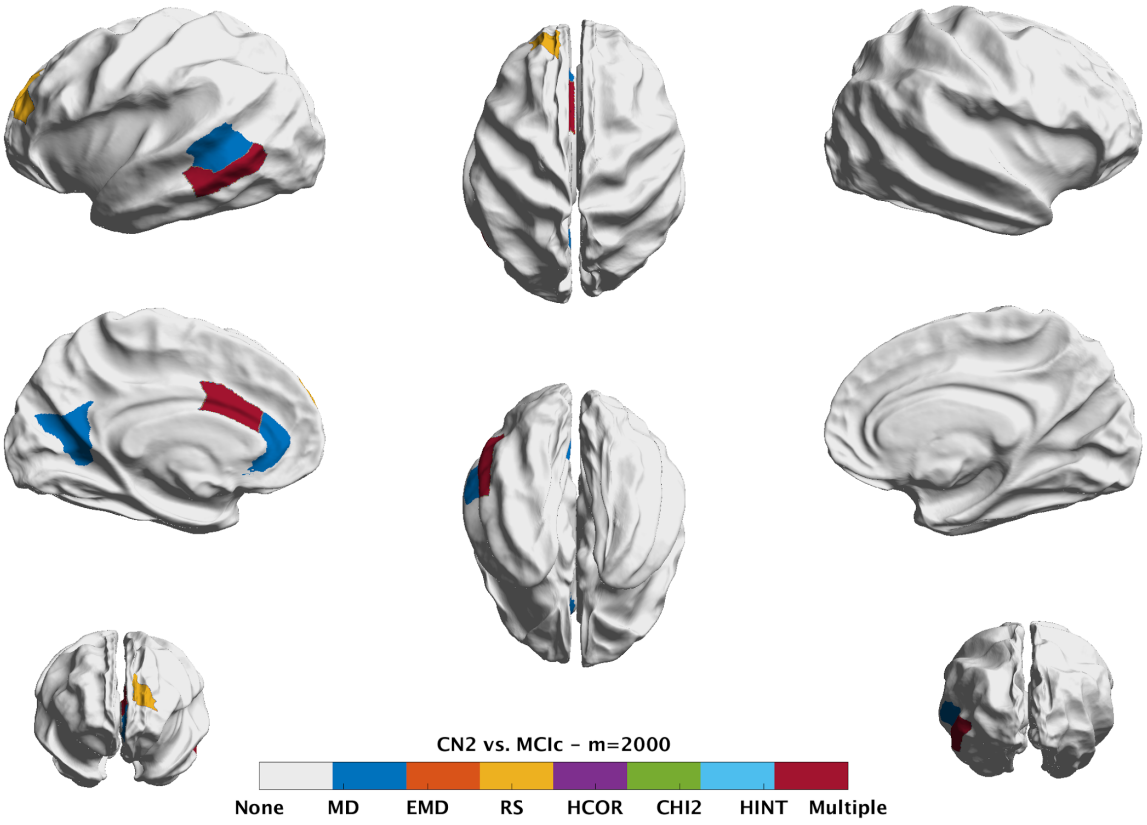

***Fig 6**: Visualization of the most discriminative regions as derived from the CN2 vs. MCIc experiment at m=2000. MDRs in this experiment identify regions in middle temporal lobe, cingulate (anterior and inferior), cuneus and precuneus, which are known to be associated with progressive MCI and prodromal AD.*

bioRxiv preprint doi: https://doi.org/10.1101/170381; this version posted July 9, 2019. The copyright holder for this preprint (which was not certified by peer review) is the author/funder, who has granted bioRxiv a license to display the preprint in perpetuity. It is made available under aCC-BY-NC-ND 4.0 International license.

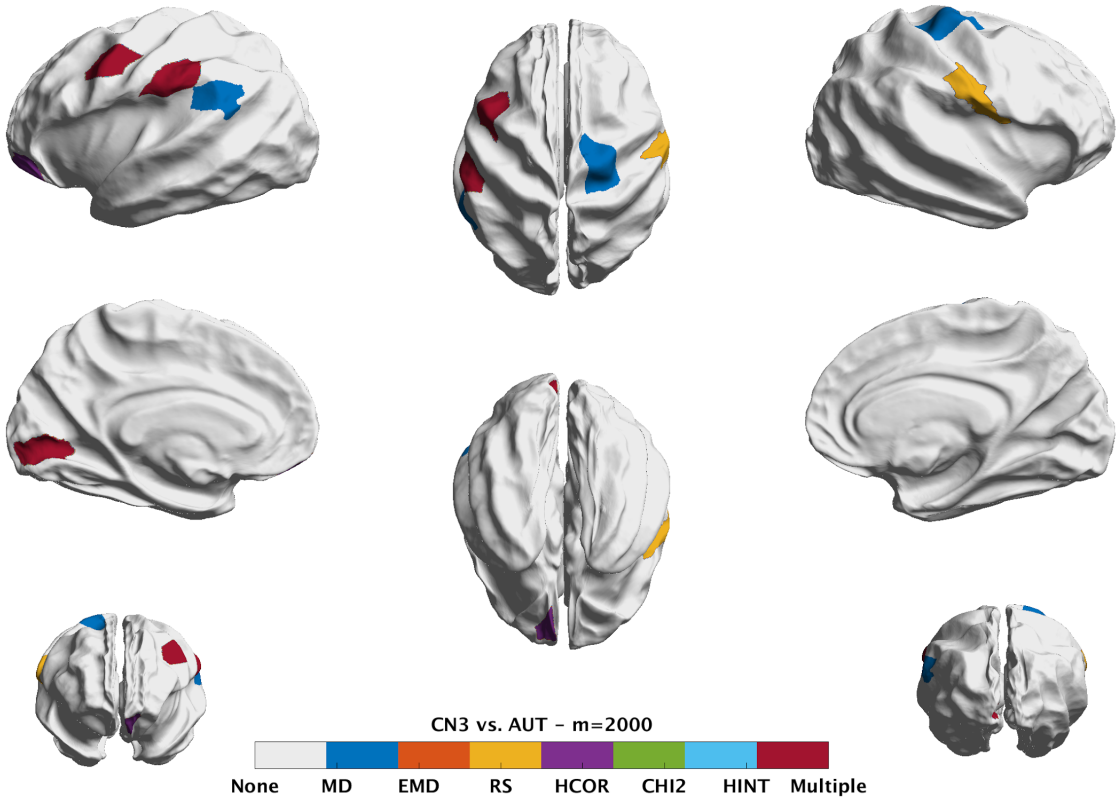

***Fig 7**: Visualization of the most discriminative regions as derived from the CN3 vs. AUT experiment at m=2000. These regions cover the lingual, supra-marginal, post- and precentral areas.*

Future directions

While we present the results from a large number (108) of experiments covering two large publicly available datasets, two disease and age groups and three different levels of separability, there is certainly room for further analysis. Future studies could consider additional histogram distances, and performing the comparison with different types of classifiers (other than SVM such as linear discriminant or random forests).

It is possible that lack of sufficiently large sample size could be a contributor to the observed lack of statistically significant differences. Especially, in challenging classification experiments such as CN3 vs. AUT. It would be ideal to evaluate the predictive performances on additional independent validation/replication datasets (such as AIBL). Such a broadening of scope for the study is not only computationally very intensive, but we believe studying the above is unlikely to change the conclusions. It would be nevertheless useful to quantitatively support it.

It would also be interesting to study the impact of different atlas choices (other than *fsaverage*, such as MNI152), parcellation (such as (Destrieux et al. 2010)) and subdivision schemes (functional or geometric or multimodal) (Eickhoff et al. 2015; Glasser et al. 2016), potential neuroimaging artifacts and confounds (Churchill et al. 2015; J. P. Lerch, van der Kouwe, and Raznahan 2017), but this would be demanding not only computationally but also in expert manpower for quality control (typically unavailable). It would also be quite interesting to replicate this study in the context of differential diagnosis (Raamana, Rosen, et al. 2014). A cross-modal comparison (Reid et al. 2015), in terms of predictive performance, with network-level features derived from modalities such as task-free fMRI would also be interesting.

bioRxiv preprint doi: https://doi.org/10.1101/170381; this version posted July 9, 2019. The copyright holder for this preprint (which was not certified by peer review) is the author/funder, who has granted bioRxiv a license to display the preprint in perpetuity. It is made available under aCC-BY-NC-ND 4.0 International license.

Conclusions

We have studied six different ways of constructing weighted networks derived from cortical thickness features, based on a novel method to derive edge weights based on histogram distances. We performed a comprehensive model comparison based on extensive cross-validation of their predictive utility and nonparametric statistical tests. This has been studies under three separabilities (ranging from pronounced, mild and to subtle differences) derived from two independent and large publicly available datasets.

Some interesting results of this study based on the individual-subject classification results are:

- the simpler methods of edge weight computation such as the difference in median thickness are as predictive as the sophisticated methods relying on the richer descriptions based on complete histograms.
- within a given method, the impact of a spatial scale m on predictive performance is not significant. The most popular way of computing edge weights in group-wise analysis i.e. histogram correlation, is shown to be the least predictive of disease-status in the context of individualized prediction via HiWeNet.

Compliance with Ethical Standards

Conflict of Interest:
The authors declare no conflict of interest.

Research involving Human Participants and/or Animals:
Not applicable.

Informed consent:
Not applicable.

Funding

PRR is partly supported by CIHR (MOP 84483 to SCS), Ontario Neurodegenerative Disease Research Initiative (ONDRI) and Canadian Biomarker Integration Network for Depression (CANBIND), and with SCS the Ontario Brain Institute (OBI), an independent non-profit corporation, funded partially by the Ontario government. The opinions, results and conclusions are those of the authors and no endorsement by the OBI is intended or should be inferred. We also thank the financial support from the *Temerty Family Foundation*.

Acknowledgements

ADNI

Data collection and sharing for this project was funded by the Alzheimer's Disease Neuroimaging Initiative (ADNI) (National Institutes of Health Grant U01 AG024904) and DOD ADNI (Department of Defense award number W81XWH-12-2-0012). ADNI is funded by the National Institute on Aging, the National Institute of Biomedical Imaging and Bioengineering, and through generous contributions from the following: AbbVie, Alzheimer's Association; Alzheimer's Drug Discovery Foundation; Araclon Biotech; BioClinica, Inc.; Biogen; Bristol-Myers Squibb Company; CereSpir, Inc.; Cogstate; Eisai Inc.; Elan Pharmaceuticals, Inc.; Eli Lilly

bioRxiv preprint doi: https://doi.org/10.1101/170381; this version posted July 9, 2019. The copyright holder for this preprint (which was not certified by peer review) is the author/funder, who has granted bioRxiv a license to display the preprint in perpetuity. It is made available under aCC-BY-NC-ND 4.0 International license.

and Company; EuroImmun; F. Hoffmann-La Roche Ltd and its affiliated company Genentech, Inc.; Fujirebio; GE Healthcare; IXICO Ltd.; Janssen Alzheimer Immunotherapy Research & Development, LLC.; Johnson & Johnson Pharmaceutical Research & Development LLC.; Lumosity; Lundbeck; Merck & Co., Inc.; Meso Scale Diagnostics, LLC.; NeuroRx Research; Neurotrack Technologies; Novartis Pharmaceuticals Corporation; Pfizer Inc.; Piramal Imaging; Servier; Takeda Pharmaceutical Company; and Transition Therapeutics. The Canadian Institutes of Health Research is providing funds to support ADNI clinical sites in Canada. Private sector contributions are facilitated by the Foundation for the National Institutes of Health (www.fnih.org). The grantee organization is the Northern California Institute for Research and Education, and the study is coordinated by the Alzheimer's Therapeutic Research Institute at the University of Southern California. ADNI data are disseminated by the Laboratory for NeuroImaging at the University of Southern California.

ABIDE I

Primary support for the work by Adriana Di Martino was provided by the NIMH (K23MH087770) and the Leon Levy Foundation. Primary support for the work by Michael P. Milham and the INDI team was provided by gifts from Joseph P. Healy and the Stavros Niarchos Foundation to the Child Mind Institute, as well as by an NIMH award to MPM (R03MH096321).

References

Abraham, Alexandre, Michael P. Milham, Adriana Di Martino, R. Cameron Craddock, Dimitris Samaras, Bertrand Thirion, and Gael Varoquaux. 2017. "Deriving Reproducible Biomarkers from Multi-Site Resting-State Data: An Autism-Based Example." *NeuroImage* 147 (February): 736–45. https://doi.org/10.1016/j.neuroimage.2016.10.045.

Alexander-Bloch, Aaron, Jay N. Giedd, and Ed Bullmore. 2013. "Imaging Structural Co-Variance between Human Brain Regions." *Nature Reviews. Neuroscience* 14 (5): 322–36. http://www.nature.com/doifinder/10.1038/nrn3465.

Alzheimer's Association. 2017. "2017 Alzheimer's Disease Facts and Figures." *Alzheimer's & Dementia: The Journal of the Alzheimer's Association* 13 (4): 325–73. https://doi.org/10.1016/j.jalz.2017.02.001.

Arbabshirani, Mohammad R., Sergey Plis, Jing Sui, and Vince D. Calhoun. 2017. "Single Subject Prediction of Brain Disorders in Neuroimaging: Promises and Pitfalls." *NeuroImage* 145 (Pt B): 137–65. http://linkinghub.elsevier.com/retrieve/pii/S105381191600210X.

Bron, Esther E., Marion Smits, Wiesje M. van der Flier, Hugo Vrenken, Frederik Barkhof, Philip Scheltens, Janne M. Papma, et al. 2015. "Standardized Evaluation of Algorithms for Computer-Aided Diagnosis of Dementia Based on Structural MRI: The CADDementia Challenge." *NeuroImage* 111 (May): 562–79. https://doi.org/10.1016/j.neuroimage.2015.01.048.

Burman, Prabir. 1989. "A Comparative Study of Ordinary Cross-Validation, v-Fold Cross-Validation and the Repeated Learning-Testing Methods." *Biometrika* 76 (3): 503–14. http://biomet.oxfordjournals.org/cgi/doi/10.1093/biomet/76.3.503.

Churchill, Nathan W., Robyn Spring, Babak Afshin-Pour, Fan Dong, and Stephen C. Strother. 2015. "An Automated, Adaptive Framework for Optimizing Preprocessing Pipelines in Task-Based Functional MRI." *PloS One* 10 (7): e0131520. http://dx.plos.org/10.1371/journal.pone.0131520.

Craddock, Cameron and Benhajali, Yassine and Chu, Carlton and Chouinard, Francois and Evans, Alan and Jakab, Andr?s and Khundrakpam, Budhachandra Singh and Lewis, John David and Li, Qingyang and Milham, Michael and Yan, Chaogan and Bellec, Pierre. 2013. "The Neuro Bureau Preprocessing Initiative: Open Sharing of Preprocessed Neuroimaging Data and Derivatives]." *Frontiers in Neuroinformatics*.

bioRxiv preprint doi: https://doi.org/10.1101/170381; this version posted July 9, 2019. The copyright holder for this preprint (which was not certified by peer review) is the author/funder, who has granted bioRxiv a license to display the preprint in perpetuity. It is made available under aCC-BY-NC-ND 4.0 International license.

https://doi.org/10.3389/conf.fninf.2013.09.00041.

Cuingnet, Rémi, Emilie Gerardin, Jérôme Tessieras, Guillaume Auzias, Stéphane Lehéricy, Marie-Odile Habert, Marie Chupin, Habib Benali, Olivier Colliot, and Alzheimer's Disease Neuroimaging Initiative. 2011. "Automatic Classification of Patients with Alzheimer's Disease from Structural MRI: A Comparison of Ten Methods Using the ADNI Database." *NeuroImage* 56 (2): 766–81. https://doi.org/10.1016/j.neuroimage.2010.06.013.

Cummings, Jeffrey L., Travis Morstorf, and Kate Zhong. 2014. "Alzheimer's Disease Drug-Development Pipeline: Few Candidates, Frequent Failures." *Alzheimer's Research & Therapy* 6 (4): 37. https://doi.org/10.1186/alzrt269.

Dai, Dai, Huiguang He, Joshua T. Vogelstein, and Zengguang Hou. 2012. "Accurate Prediction of AD Patients Using Cortical Thickness Networks." *International Journal of Computer Vision*, October. http://www.springerlink.com/index/10.1007/s00138-012-0462-0.

Demšar, Janez. 2006. "Statistical Comparisons of Classifiers over Multiple Data Sets." *Journal of Machine Learning Research: JMLR* 7 (January): 1–30. http://dl.acm.org/citation.cfm?id=1248548.

Destrieux, Christophe, Bruce Fischl, Anders Dale, and Eric Halgren. 2010. "Automatic Parcellation of Human Cortical Gyri and Sulci Using Standard Anatomical Nomenclature." *NeuroImage* 53 (1): 1–15. https://doi.org/10.1016/j.neuroimage.2010.06.010.

Dickerson, B. C., E. Fenstermacher, D. H. Salat, D. A. Wolk, R. P. Maguire, R. Desikan, J. Pacheco, et al. 2008. "Detection of Cortical Thickness Correlates of Cognitive Performance: Reliability across MRI Scan Sessions, Scanners, and Field Strengths." *NeuroImage* 39 (1): 10–18. https://doi.org/10.1016/j.neuroimage.2007.08.042.

Dietterich, Thomas G. 1998. "Approximate Statistical Tests for Comparing Supervised Classification Learning Algorithms." *Neural Computation* 10 (7): 1895–1923. http://www.mitpressjournals.org/doi/abs/10.1162/089976698300017197.

Duchesne, S., A. Caroli, C. Geroldi, and C. Barillot. 2008. "MRI-Based Automated Computer Classification of Probable AD versus Normal Controls." *IEEE Transactions on Medical Imaging*, January. http://ieeexplore.ieee.org/xpls/abs_all.jsp?arnumber=4479633.

Dukart, Juergen, Karsten Mueller, Annette Horstmann, Henryk Barthel, Harald E. Möller, Arno Villringer, Osama Sabri, and Matthias L. Schroeter. 2011. "Combined Evaluation of FDG-PET and MRI Improves Detection and Differentiation of Dementia." *PloS One* 6 (3): e18111. http://dx.plos.org/10.1371/journal.pone.0018111.

Dyrba, M., Barkhof, F., Fellgiebel, A., Filippi, M., Hausner, L., Hauenstein, K., Kirste, T. and Teipel, S.J. 2015. "Predicting Prodromal Alzheimer's Disease in Subjects with Mild Cognitive Impairment Using Machine Learning Classification of Multimodal Multicenter Diffusion- …." *Journal of Neuroimaging* 25 (5): 738–47. http://onlinelibrary.wiley.com/doi/10.1111/jon.12214/full.

Eickhoff, Simon B., Bertrand Thirion, Gaël Varoquaux, and Danilo Bzdok. 2015. "Connectivity-based Parcellation: Critique and Implications." *Human Brain Mapping* 36 (12): 4771–92. http://onlinelibrary.wiley.com.myaccess.library.utoronto.ca/doi/10.1002/hbm.22933/full.

Evans, Alan C. 2013. "Networks of Anatomical Covariance." *NeuroImage* 80 (October): 489–504. http://eutils.ncbi.nlm.nih.gov/entrez/eutils/elink.fcgi?dbfrom=pubmed&id=23711536&retmode=ref&cmd=prlinks.

Fischl, B., and A. Dale. 2000. "Measuring the Thickness of the Human Cerebral Cortex from Magnetic Resonance Images." *Proceedings of the National Academy of Sciences*, January. http://www.pnas.org/cgi/content/abstract/97/20/11050.

Fischl, Bruce, David H. Salat, Evelina Busa, Marilyn Albert, Megan Dieterich, Christian Haselgrove, Andre van der Kouwe, et al. 2002. "Whole Brain Segmentation:: Automated Labeling of Neuroanatomical Structures in the Human Brain." *Neuron* 33 (3): 341–55. https://doi.org/10.1016/S0896-6273(02)00569-X.

Glasser, Matthew F., Timothy S. Coalson, Emma C. Robinson, Carl D. Hacker, John Harwell, Essa Yacoub, Kamil Ugurbil, et al. 2016. "A Multi-Modal Parcellation of Human Cerebral Cortex." *Nature* 536 (7615): 171–78. https://doi.org/10.1038/nature18933.

Gong, Gaolang, Yong He, Zhang J. Chen, and Alan C. Evans. 2012. "Convergence and Divergence of Thickness Correlations with Diffusion Connections across the Human

bioRxiv preprint doi: https://doi.org/10.1101/170381; this version posted July 9, 2019. The copyright holder for this preprint (which was not certified by peer review) is the author/funder, who has granted bioRxiv a license to display the preprint in perpetuity. It is made available under aCC-BY-NC-ND 4.0 International license.

Cerebral Cortex." *NeuroImage* 59 (2): 1239–48. http://www.sciencedirect.com/science/article/pii/S1053811911009049.

Han, Xiao, Jorge Jovicich, David Salat, Andre van der Kouwe, Brian Quinn, Silvester Czanner, Evelina Busa, et al. 2006. "Reliability of MRI-Derived Measurements of Human Cerebral Cortical Thickness: The Effects of Field Strength, Scanner Upgrade and Manufacturer." *NeuroImage* 32 (1): 180–94. http://linkinghub.elsevier.com/retrieve/pii/S1053811906001601.

Herholz, K., E. Salmon, D. Perani, J-C Baron, V. Holthoff, L. Frölich, P. Schönknecht, K. Ito, R. Mielke, and E. Kalbe. 2002. "Discrimination between Alzheimer Dementia and Controls by Automated Analysis of Multicenter FDG PET." *NeuroImage* 17 (1): 302–16. http://linkinghub.elsevier.com/retrieve/pii/S1053811902912085.

He, Y., and Z. Chen. 2007. "Small-World Anatomical Networks in the Human Brain Revealed by Cortical Thickness from MRI." *Cerebral Cortex* , January. http://cercor.oxfordjournals.org/content/17/10/2407.abstract.

Hojjati, S. H., A. Ebrahimzadeh, and A. Khazaee. 2017. "Predicting Conversion from MCI to AD Using Resting-State fMRI, Graph Theoretical Approach and SVM." *Journal of Neuroscience*. http://www.sciencedirect.com/science/article/pii/S0165027017300638.

Iscan, Zafer, Tony B. Jin, Alexandria Kendrick, Bryan Szeglin, Hanzhang Lu, Madhukar Trivedi, Maurizio Fava, et al. 2015. "Test-Retest Reliability of Freesurfer Measurements within and between Sites: Effects of Visual Approval Process." *Human Brain Mapping* 36 (9): 3472–85. https://doi.org/10.1002/hbm.22856.

Jack, Clifford R., Jr, Matt A. Bernstein, Nick C. Fox, Paul Thompson, Gene Alexander, Danielle Harvey, Bret Borowski, et al. 2008. "The Alzheimer's Disease Neuroimaging Initiative (ADNI): MRI Methods." *Journal of Magnetic Resonance Imaging: JMRI* 27 (4): 685–91. https://doi.org/10.1002/jmri.21049.

Kim, Hee-Jong, Jeong-Hyeon Shin, Cheol E. Han, Hee Jin Kim, Duk L. Na, Sang Won Seo, Joon-Kyung Seong, and Alzheimer's Disease Neuroimaging Initiative. 2016. "Using Individualized Brain Network for Analyzing Structural Covariance of the Cerebral Cortex in Alzheimer's Patients." *Frontiers in Neuroscience* 10 (September): 394. https://doi.org/10.3389/fnins.2016.00394.

Kourentzes, Nikolaos. 2016. "ANOM and Nemenyi Tests." 2016. http://kourentzes.com/forecasting/2013/04/19/nemenyi-test/.

Lerch, Jason P., Keith Worsley, W. Philip Shaw, Deanna K. Greenstein, Rhoshel K. Lenroot, Jay Giedd, and Alan C. Evans. 2006. "Mapping Anatomical Correlations across Cerebral Cortex (MACACC) Using Cortical Thickness from MRI." *NeuroImage* 31 (3): 993–1003. http://linkinghub.elsevier.com/retrieve/pii/S1053811906000425.

Lerch, J. P., Ajw van der Kouwe, and A. Raznahan. 2017. "Studying Neuroanatomy Using MRI." *Nature*. http://www.nature.com/neuro/journal/v20/n3/abs/nn.4501.html.

Matthews, Dawn C., Ana S. Lukic, Randolph D. Andrews, Boris Marendic, James Brewer, Robert A. Rissman, Lisa Mosconi, et al. 2016. "Dissociation of Down Syndrome and Alzheimer's Disease Effects with Imaging." *Alzheimer's & Dementia: The Journal of the Alzheimer's Association* 2 (2): 69–81. https://doi.org/10.1016/j.trci.2016.02.004.

Moradi, Elaheh, Budhachandra Khundrakpam, John D. Lewis, Alan C. Evans, and Jussi Tohka. 2017. "Predicting Symptom Severity in Autism Spectrum Disorder Based on Cortical Thickness Measures in Agglomerative Data." *NeuroImage* 144 (Pt A): 128–41. https://doi.org/10.1016/j.neuroimage.2016.09.049.

Phillips, David J., Alec McGlaughlin, David Ruth, Leah R. Jager, and Anja Soldan. 2015. "Graph Theoretic Analysis of Structural Connectivity across the Spectrum of Alzheimer's Disease: The Importance of Graph Creation Methods." *NeuroImage: Clinical* 7 (January): 377–90. http://linkinghub.elsevier.com/retrieve/pii/S221315821500008X.

Power, Jonathan D., Alexander L. Cohen, Steven M. Nelson, Gagan S. Wig, Kelly Anne Barnes, Jessica A. Church, Alecia C. Vogel, et al. 2011. "Functional Network Organization of the Human Brain." *Neuron* 72 (4): 665–78. https://doi.org/10.1016/j.neuron.2011.09.006.

Raamana, Pradeep Reddy. 2017. *Neuropredict: Easy Machine Learning and Standardized Predictive Analysis of Biomarkers*. https://doi.org/10.5281/zenodo.1058993.

bioRxiv preprint doi: https://doi.org/10.1101/170381; this version posted July 9, 2019. The copyright holder for this preprint (which was not certified by peer review) is the author/funder, who has granted bioRxiv a license to display the preprint in perpetuity. It is made available under aCC-BY-NC-ND 4.0 International license.

Raamana, Pradeep Reddy, Howard Rosen, Bruce Miller, Michael W. Weiner, Lei Wang, and Mirza Faisal Beg. 2014. "Three-Class Differential Diagnosis among Alzheimer Disease, Frontotemporal Dementia and Controls." *Frontiers in Neurology* 5 (71): 71. https://doi.org/10.3389/fneur.2014.00071.

Raamana, Pradeep Reddy, and Stephen Strother. 2018. "Graynet: Single-Subject Morphometric Networks for Neuroscience Connectivity Applications." *Journal of Open Source Software* 3 (30): 924. https://doi.org/10.21105/joss.00924.

Raamana, Pradeep Reddy, and Stephen C. Strother. 2017. "Histogram-Weighted Networks for Feature Extraction, Connectivity and Advanced Analysis in Neuroscience." *The Journal of Open Source Software* 2 (19): 380. https://doi.org/10.21105/joss.00380.

Raamana, Pradeep Reddy, Michael W. Weiner, Lei Wang, and Mirza Faisal Beg. 2015. "Thickness Network Features for Prognostic Applications in Dementia." *Neurobiology of Aging* 36 (January): S91–102. http://linkinghub.elsevier.com/retrieve/pii/S0197458014005521.

Raamana, Pradeep Reddy, Wei Wen, Nicole A. Kochan, Henry Brodaty, Perminder S. Sachdev, Lei Wang, and Mirza Faisal Beg. 2014. "Novel ThickNet Features for the Discrimination of Amnestic MCI Subtypes." *NeuroImage: Clinical* 6 (January): 284–95. http://www.sciencedirect.com/science/article/pii/S2213158214001417.

Reid, Andrew T., and Alan C. Evans. 2013. "Structural Networks in Alzheimer's Disease." *European Neuropsychopharmacology: The Journal of the European College of Neuropsychopharmacology* 23 (1): 63–77. http://linkinghub.elsevier.com/retrieve/pii/S0924977X12003227.

Reid, Andrew T., John Lewis, Gleb Bezgin, Budhachandra Khundrakpam, Simon B. Eickhoff, Anthony R. McIntosh, Pierre Bellec, and Alan C. Evans. 2015. "A Cross-Modal, Cross-Species Comparison of Connectivity Measures in the Primate Brain." *NeuroImage*, October. http://linkinghub.elsevier.com/retrieve/pii/S1053811915009696.

Scheel, Christian, Anna Rotarska-Jagiela, Leonhard Schilbach, Fritz G. Lehnhardt, Barbara Krug, Kai Vogeley, and Ralf Tepest. 2011. "Imaging Derived Cortical Thickness Reduction in High-Functioning Autism: Key Regions and Temporal Slope." *NeuroImage* 58 (2): 391–400. https://doi.org/10.1016/j.neuroimage.2011.06.040.

Seidlitz, Jakob, František Váša, Maxwell Shinn, Rafael Romero-Garcia, Kirstie J. Whitaker, Petra E. Vértes, Paul Kirkpatrick Reardon, et al. 2017. "Morphometric Similarity Networks Detect Microscale Cortical Organisation And Predict Inter-Individual Cognitive Variation." *bioRxiv*. https://doi.org/10.1101/135855.

Smith, Elizabeth, Audrey Thurm, Deanna Greenstein, Cristan Farmer, Susan Swedo, Jay Giedd, and Armin Raznahan. 2016. "Cortical Thickness Change in Autism during Early Childhood." *Human Brain Mapping* 37 (7): 2616–29. https://doi.org/10.1002/hbm.23195.

Spreng, R. Nathan, Jorge Sepulcre, Gary R. Turner, W. Dale Stevens, and Daniel L. Schacter. 2013. "Intrinsic Architecture Underlying the Relations among the Default, Dorsal Attention, and Frontoparietal Control Networks of the Human Brain." *Journal of Cognitive Neuroscience* 25 (1): 74–86. https://doi.org/10.1162/jocn_a_00281.

Spreng, R. Nathan, and Gary R. Turner. 2013. "Structural Covariance of the Default Network in Healthy and Pathological Aging." *The Journal of Neuroscience: The Official Journal of the Society for Neuroscience* 33 (38): 15226–34. http://www.jneurosci.org.proxy.lib.sfu.ca/content/33/38/15226.full.

Stam, Cornelis J. 2014. "Modern Network Science of Neurological Disorders." *Nature Reviews. Neuroscience* 15 (10): 683–95. http://www.nature.com/doifinder/10.1038/nrn3801.

Sui, J., T. Adali, Q. Yu, and J. Chen. 2011. "A Review of Multivariate Methods for Multimodal Fusion of Brain Imaging Data." *Journal of Neuroscience Methods*, January. http://www.sciencedirect.com/science/article/pii/S0165027011006820.

Tijms, Betty M., Peggy Seriès, David J. Willshaw, and Stephen M. Lawrie. 2012. "Similarity-Based Extraction of Individual Networks from Gray Matter MRI Scans." *Cerebral Cortex* 22 (7): 1530–41. http://eutils.ncbi.nlm.nih.gov/entrez/eutils/elink.fcgi?dbfrom=pubmed&id=21878484&retmode=ref&cmd=prlinks.

bioRxiv preprint doi: https://doi.org/10.1101/170381; this version posted July 9, 2019. The copyright holder for this preprint (which was not certified by peer review) is the author/funder, who has granted bioRxiv a license to display the preprint in perpetuity. It is made available under aCC-BY-NC-ND 4.0 International license.

Tijms, Betty M., Alle Meije Wink, Willem de Haan, Wiesje M. van der Flier, Cornelis J. Stam, Philip Scheltens, and Frederik Barkhof. 2013. "Alzheimer's Disease: Connecting Findings from Graph Theoretical Studies of Brain Networks." *Neurobiology of Aging* 34 (8): 2023–36. http://eutils.ncbi.nlm.nih.gov/entrez/eutils/elink.fcgi?dbfrom=pubmed&id=23541878&retmode=ref&cmd=prlinks.

Varoquaux, Gaël, Pradeep Reddy Raamana, Denis A. Engemann, Andrés Hoyos-Idrobo, Yannick Schwartz, and Bertrand Thirion. 2016. "Assessing and Tuning Brain Decoders: Cross-Validation, Caveats, and Guidelines." *NeuroImage*, October. http://linkinghub.elsevier.com/retrieve/pii/S105381191630595X.

Wee, Chong-Yaw, Pew-Thian Yap, Dinggang Shen, and for the Alzheimer's Disease Neuroimaging Initiative. 2012. "Prediction of Alzheimer's Disease and Mild Cognitive Impairment Using Cortical Morphological Patterns." *Human Brain Mapping*, August. http://eutils.ncbi.nlm.nih.gov/entrez/eutils/elink.fcgi?dbfrom=pubmed&id=22927119&retmode=ref&cmd=prlinks.

Weiner, Michael W., Dallas P. Veitch, Paul S. Aisen, Laurel A. Beckett, Nigel J. Cairns, Jesse Cedarbaum, Robert C. Green, et al. 2015. "2014 Update of the Alzheimer's Disease Neuroimaging Initiative: A Review of Papers Published since Its Inception." *Alzheimer's and Dementia* 11 (6): e1–120. http://linkinghub.elsevier.com/retrieve/pii/S1552526014028659.

Weiner, Michael W., Dallas P. Veitch, Paul S. Aisen, Laurel A. Beckett, Nigel J. Cairns, Robert C. Green, Danielle Harvey, et al. 2013. "The Alzheimer's Disease Neuroimaging Initiative: A Review of Papers Published since Its Inception." *Alzheimer's & Dementia: The Journal of the Alzheimer's Association* 9 (5): e111–94. http://linkinghub.elsevier.com/retrieve/pii/S1552526013024291.

———. 2017. "Recent Publications from the Alzheimer's Disease Neuroimaging Initiative: Reviewing Progress toward Improved AD Clinical Trials." *Alzheimer's & Dementia: The Journal of the Alzheimer's Association*. https://doi.org/10.1016/j.jalz.2016.11.007.

Wen, Wei, Yong He, and Perminder Sachdev. 2011. "Structural Brain Networks and Neuropsychiatric Disorders." *Current Opinion in Psychiatry* 24 (3): 219–25. http://content.wkhealth.com/linkback/openurl?sid=WKPTLP:landingpage&an=00001504-201105000-00009.

Wijk, Bernadette C. M. van, Cornelis J. Stam, and Andreas Daffertshofer. 2010. "Comparing Brain Networks of Different Size and Connectivity Density Using Graph Theory." *PloS One* 5 (10): e13701. http://dx.plos.org/10.1371/journal.pone.0013701.

Zalesky, Andrew, Alex Fornito, Ian H. Harding, Luca Cocchi, Murat Yücel, Christos Pantelis, and Edward T. Bullmore. 2010. "Whole-Brain Anatomical Networks: Does the Choice of Nodes Matter?" *NeuroImage* 50 (3): 970–83. http://linkinghub.elsevier.com/retrieve/pii/S1053811909013159.

Supplementary material

Appendix A - Details of subjects used in this study.

Subject IDs from ADNI in Table 1

Note these subjects are all from baseline.

AD from Table 1

011_S_0003	128_S_0310	018_S_0633	126_S_0891	109_S_1157	127_S_1382	005_S_0814
022_S_0007	031_S_0321	021_S_0642	023_S_0916	013_S_1161	027_S_1385	002_S_0816
011_S_0010	035_S_0341	006_S_0653	005_S_0929	094_S_1164	094_S_1397	137_S_0841
067_S_0029	021_S_0343	018_S_0682	002_S_0955	133_S_1170	128_S_1409	127_S_0844

bioRxiv preprint doi: https://doi.org/10.1101/170381; this version posted July 9, 2019. The copyright holder for this preprint (which was not certified by peer review) is the author/funder, who has granted bioRxiv a license to display the preprint in perpetuity. It is made available under aCC-BY-NC-ND 4.0 International license.

011_S_0053	137_S_0366	012_S_0689	114_S_0979	024_S_1171	041_S_1435	098_S_0884
067_S_0076	116_S_0370	012_S_0712	016_S_0991	067_S_1185	023_S_0078	002_S_0938
023_S_0083	114_S_0374	012_S_0720	100_S_0995	109_S_1192	098_S_0149	130_S_0956
023_S_0084	116_S_0392	033_S_0733	013_S_0996	013_S_1205	128_S_0167	029_S_0999
123_S_0088	032_S_0400	128_S_0740	036_S_1001	126_S_1221	100_S_0190	094_S_1027
123_S_0091	027_S_0404	100_S_0747	002_S_1018	067_S_1253	128_S_0216	027_S_1081
023_S_0093	136_S_0426	021_S_0753	141_S_1024	027_S_1254	022_S_0219	094_S_1090
123_S_0094	127_S_0431	127_S_0754	032_S_1037	003_S_1257	007_S_0316	014_S_1095
068_S_0109	137_S_0438	036_S_0759	137_S_1041	023_S_1262	014_S_0328	100_S_1113
067_S_0110	099_S_0470	036_S_0760	053_S_1044	016_S_1263	018_S_0335	029_S_1184
022_S_0129	116_S_0487	109_S_0777	133_S_1055	033_S_1281	014_S_0356	130_S_1201
023_S_0139	099_S_0492	010_S_0786	029_S_1056	033_S_1283	099_S_0372	031_S_1209
032_S_0147	131_S_0497	141_S_0790	003_S_1059	033_S_1285	057_S_0474	007_S_1248
123_S_0162	128_S_0517	062_S_0793	100_S_1062	023_S_1289	073_S_0565	007_S_1304
011_S_0183	128_S_0528	012_S_0803	082_S_1079	130_S_1290	037_S_0627	009_S_1334
136_S_0194	062_S_0535	067_S_0812	027_S_1082	051_S_1296	062_S_0690	007_S_1339
020_S_0213	022_S_0543	067_S_0828	032_S_1101	024_S_1307	131_S_0691	005_S_1341
005_S_0221	006_S_0547	010_S_0829	094_S_1102	033_S_1308	141_S_0696	057_S_1371
114_S_0228	031_S_0554	029_S_0836	021_S_1109	130_S_1337	013_S_0699	057_S_1379
128_S_0266	036_S_0577	027_S_0850	141_S_1137	009_S_1354	033_S_0724	041_S_1391
018_S_0286	013_S_0592	141_S_0852	099_S_1144	041_S_1368	062_S_0730	094_S_1402
136_S_0299	126_S_0606	141_S_0853	141_S_1152	057_S_1373	100_S_0743	128_S_1430
136_S_0300	002_S_0619	033_S_0889	100_S_1154	082_S_1377	126_S_0784	

CN1 subjects used in Table 1

011_S_0002	123_S_0106	073_S_0312	013_S_0502	127_S_0684	003_S_0931	116_S_1249
011_S_0005	123_S_0113	072_S_0315	126_S_0506	002_S_0685	057_S_0934	052_S_1250
011_S_0008	027_S_0120	131_S_0319	033_S_0516	137_S_0686	052_S_0951	052_S_1251
022_S_0014	131_S_0123	037_S_0327	014_S_0519	094_S_0692	023_S_0963	082_S_1256
100_S_0015	041_S_0125	021_S_0337	128_S_0522	141_S_0717	109_S_0967	002_S_1261
011_S_0016	068_S_0127	099_S_0352	133_S_0525	141_S_0726	130_S_0969	094_S_1267
067_S_0019	035_S_0156	016_S_0359	094_S_0526	006_S_0731	137_S_0972	013_S_1276
011_S_0021	021_S_0159	116_S_0360	099_S_0534	033_S_0734	041_S_1002	002_S_1280
011_S_0022	114_S_0166	082_S_0363	016_S_0538	033_S_0741	012_S_1009	100_S_1286
011_S_0023	098_S_0171	018_S_0369	128_S_0545	009_S_0751	109_S_1013	020_S_1288
023_S_0031	098_S_0172	116_S_0382	014_S_0548	082_S_0761	109_S_1014	131_S_1301
100_S_0035	114_S_0173	073_S_0386	035_S_0555	141_S_0767	033_S_1016	035_S_0048

bioRxiv preprint doi: https://doi.org/10.1101/170381; this version posted July 9, 2019. The copyright holder for this preprint (which was not certified by peer review) is the author/funder, who has granted bioRxiv a license to display the preprint in perpetuity. It is made available under aCC-BY-NC-ND 4.0 International license.

099_S_0040	067_S_0177	027_S_0403	014_S_0558	062_S_0768	036_S_1023	022_S_0066
018_S_0043	136_S_0184	126_S_0405	002_S_0559	057_S_0779	024_S_1063	022_S_0130
100_S_0047	136_S_0186	002_S_0413	013_S_0575	141_S_0810	033_S_1086	136_S_0196
067_S_0056	068_S_0210	114_S_0416	036_S_0576	036_S_0813	141_S_1094	073_S_0311
023_S_0058	005_S_0223	010_S_0419	062_S_0578	057_S_0818	033_S_1098	131_S_0441
067_S_0059	128_S_0229	010_S_0420	114_S_0601	009_S_0842	051_S_1123	014_S_0520
023_S_0061	128_S_0230	018_S_0425	005_S_0602	029_S_0843	012_S_1133	005_S_0553
010_S_0067	130_S_0232	133_S_0433	126_S_0605	029_S_0845	032_S_1169	116_S_0648
007_S_0068	128_S_0245	131_S_0436	005_S_0610	009_S_0862	023_S_1190	094_S_0711
100_S_0069	067_S_0257	037_S_0454	031_S_0618	128_S_0863	068_S_1191	129_S_0778
007_S_0070	127_S_0259	137_S_0459	127_S_0622	029_S_0866	941_S_1194	029_S_0824
123_S_0072	127_S_0260	037_S_0467	012_S_0637	109_S_0876	941_S_1195	003_S_0907
027_S_0074	041_S_0262	010_S_0472	082_S_0640	020_S_0883	941_S_1197	003_S_0981
023_S_0081	128_S_0272	032_S_0479	057_S_0643	130_S_0886	941_S_1202	021_S_0984
136_S_0086	137_S_0283	006_S_0484	021_S_0647	098_S_0896	941_S_1203	024_S_0985
073_S_0089	002_S_0295	133_S_0488	116_S_0657	041_S_0898	007_S_1206	003_S_1021
099_S_0090	123_S_0298	094_S_0489	036_S_0672	020_S_0899	007_S_1222	062_S_1099
032_S_0095	137_S_0301	133_S_0493	032_S_0677	033_S_0920	116_S_1232	130_S_1200
022_S_0096	037_S_0303	006_S_0498	126_S_0680	033_S_0923	094_S_1241	012_S_1212
020_S_0097	082_S_0304	128_S_0500	006_S_0681	023_S_0926	128_S_1242	023_S_1306

MCIc subjects used in Table 1

002_S_0954	023_S_0042	035_S_0204	127_S_0394	011_S_0861	041_S_0549	126_S_1077
002_S_1070	023_S_0388	035_S_0997	133_S_0638	011_S_1282	041_S_1412	127_S_1427
005_S_0222	023_S_0604	051_S_1331	136_S_0195	013_S_0325	041_S_1423	128_S_0947
007_S_0041	023_S_0855	052_S_0952	141_S_0982	014_S_0658	057_S_0941	130_S_0423
007_S_0128	023_S_0887	052_S_1054	941_S_1311	023_S_0030	057_S_1217	133_S_0727
007_S_0344	023_S_1247	053_S_0507	941_S_1363	023_S_0625	067_S_0045	133_S_0913
011_S_0856	027_S_0461	062_S_1299	002_S_0729	027_S_0179	067_S_0077	136_S_0695
013_S_0240	033_S_0723	067_S_0243	005_S_0572	027_S_0256	094_S_0434	141_S_0915
013_S_0860	033_S_0725	067_S_0336	006_S_1130	027_S_1213	098_S_0269	141_S_1244
022_S_0750	033_S_0906	094_S_1015	007_S_0249	027_S_1387	099_S_0054	941_S_1295
022_S_1394	033_S_0922	094_S_1398	011_S_0241	033_S_0567	099_S_0111	

bioRxiv preprint doi: https://doi.org/10.1101/170381; this version posted July 9, 2019. The copyright holder for this preprint (which was not certified by peer review) is the author/funder, who has granted bioRxiv a license to display the preprint in perpetuity. It is made available under aCC-BY-NC-ND 4.0 International license.

CN2 subjects used in Table 1

011_S_0002	020_S_0097	073_S_0386	002_S_0559	062_S_0768	041_S_1002	013_S_1276
011_S_0005	027_S_0120	027_S_0403	013_S_0575	057_S_0779	109_S_1013	002_S_1280
011_S_0008	131_S_0123	126_S_0405	036_S_0576	141_S_0810	109_S_1014	020_S_1288
022_S_0014	041_S_0125	002_S_0413	062_S_0578	036_S_0813	033_S_1016	131_S_1301
011_S_0016	035_S_0156	114_S_0416	114_S_0601	029_S_0843	036_S_1023	035_S_0048
067_S_0019	114_S_0166	133_S_0433	005_S_0602	029_S_0845	024_S_1063	022_S_0066
011_S_0021	098_S_0171	131_S_0436	126_S_0605	128_S_0863	033_S_1086	022_S_0130
011_S_0022	098_S_0172	006_S_0484	005_S_0610	029_S_0866	141_S_1094	136_S_0196
011_S_0023	114_S_0173	133_S_0488	127_S_0622	109_S_0876	033_S_1098	073_S_0311
023_S_0031	067_S_0177	094_S_0489	082_S_0640	020_S_0883	051_S_1123	131_S_0441
099_S_0040	136_S_0184	133_S_0493	057_S_0643	130_S_0886	023_S_1190	014_S_0520
067_S_0056	136_S_0186	006_S_0498	036_S_0672	098_S_0896	941_S_1194	005_S_0553
023_S_0058	130_S_0232	013_S_0502	126_S_0680	041_S_0898	941_S_1195	094_S_0711
067_S_0059	067_S_0257	126_S_0506	006_S_0681	020_S_0899	941_S_1197	029_S_0824
023_S_0061	127_S_0259	033_S_0516	127_S_0684	033_S_0920	941_S_1202	003_S_0907
007_S_0068	127_S_0260	014_S_0519	002_S_0685	033_S_0923	941_S_1203	003_S_0981
007_S_0070	002_S_0295	133_S_0525	094_S_0692	023_S_0926	007_S_1206	024_S_0985
027_S_0074	082_S_0304	094_S_0526	141_S_0717	003_S_0931	007_S_1222	003_S_1021
023_S_0081	073_S_0312	099_S_0534	006_S_0731	057_S_0934	052_S_1250	062_S_1099
136_S_0086	131_S_0319	016_S_0538	033_S_0734	052_S_0951	052_S_1251	130_S_1200
073_S_0089	099_S_0352	014_S_0548	033_S_0741	023_S_0963	082_S_1256	023_S_1306
099_S_0090	016_S_0359	035_S_0555	082_S_0761	109_S_0967	002_S_1261	
022_S_0096	082_S_0363	014_S_0558	141_S_0767	130_S_0969	094_S_1267	

Subject IDs excluded from the ADNI cohort

owing to failure in Freesurfer processing or other errors

006_S_0322	018_S_0277	062_S_1091	109_S_0840
006_S_0521	027_S_0948	067_S_0020	128_S_0701
010_S_0662	027_S_1335	067_S_0024	128_S_0805
010_S_0788	031_S_0773	073_S_1207	128_S_1181
011_S_0326	033_S_0888	094_S_0964	130_S_0460
014_S_0357	033_S_1087	100_S_0893	141_S_0340

bioRxiv preprint doi: https://doi.org/10.1101/170381; this version posted July 9, 2019. The copyright holder for this preprint (which was not certified by peer review) is the author/funder, who has granted bioRxiv a license to display the preprint in perpetuity. It is made available under aCC-BY-NC-ND 4.0 International license.

Subjects IDs used from ABIDE in this study

CN3 subjects used in Table 2

Pitt_0050038	Pitt_0050047	UM_2_0050428	UCLA_1_0051281	KKI_0050776
Pitt_0050039	Pitt_0050046	UM_2_0050426	Caltech_0051484	UM_1_0050334
NYU_0051036	Trinity_0051142	UM_2_0050424	SBL_0051562	UM_1_0050335
Pitt_0050034	Leuven_1_0050703	Leuven_2_0050730	NYU_0051090	Yale_0050577
Pitt_0050035	Leuven_1_0050701	Leuven_2_0050731	Leuven_1_0050699	SBL_0051566
Pitt_0050036	NYU_0051105	Leuven_2_0050732	NYU_0051039	NYU_0051041
Pitt_0050037	NYU_0051104	Leuven_2_0050733	UM_2_0050417	Yale_0050558
Pitt_0050030	NYU_0051107	Leuven_2_0050735	Olin_0050122	UM_1_0050366
Pitt_0050031	NYU_0051106	Leuven_2_0050736	Yale_0050553	Trinity_0051137
Pitt_0050032	NYU_0051101	Leuven_2_0050737	Olin_0050109	Pitt_0050050
Pitt_0050033	NYU_0051100	Leuven_2_0050738	SBL_0051561	UCLA_2_0051309
Pitt_0050049	NYU_0051103	Leuven_2_0050739	Trinity_0051141	UCLA_2_0051306
Pitt_0050048	NYU_0051102	MaxMun_a_0051370	UM_2_0050414	UCLA_1_0051272
NYU_0051038	NYU_0051109	Leuven_2_0050741	Leuven_2_0050722	NYU_0051079
Pitt_0050041	KKI_0050782	Leuven_2_0050740	UM_2_0050422	USM_0050436
Pitt_0050040	USM_0050463	Leuven_2_0050742	UM_2_0050421	USM_0050433
Pitt_0050043	USM_0050466	Trinity_0050257	UM_2_0050427	Olin_0050119
Pitt_0050042	USM_0050467	KKI_0050820	UM_2_0050425	Trinity_0050266
Pitt_0050045	USM_0050468	SBL_0051567	NYU_0051129	SDSU_0050196
Pitt_0050044	USM_0050469	SBL_0051564	NYU_0051084	Olin_0050113

AUT subjects used in Table 2

NYU_0051032	UM_1_0050296	UCLA_1_0051224	MaxMun_d_0051350	UM_1_0050326
NYU_0051034	Pitt_0050028	UCLA_1_0051225	NYU_0050985	NYU_0050984
UCLA_1_0051240	Pitt_0050027	UCLA_1_0051226	USM_0050523	Leuven_2_0050753
Leuven_1_0050702	NYU_0051028	USM_0050488	NYU_0050994	Leuven_2_0050751
USM_0050509	Leuven_1_0050694	USM_0050487	NYU_0050997	Leuven_2_0050757
USM_0050505	CMU_a_0050654	Leuven_2_0050748	NYU_0051008	Leuven_2_0050754
USM_0050501	Leuven_1_0050711	KKI_0050801	NYU_0051009	NYU_0050954
USM_0050500	USM_0050518	KKI_0050802	NYU_0051006	NYU_0050956

bioRxiv preprint doi: https://doi.org/10.1101/170381; this version posted July 9, 2019. The copyright holder for this preprint (which was not certified by peer review) is the author/funder, who has granted bioRxiv a license to display the preprint in perpetuity. It is made available under aCC-BY-NC-ND 4.0 International license.

UM_1_0050315	UM_1_0050278	KKI_0050804	NYU_0051007	UCLA_2_0051302
Leuven_2_0050746	UM_1_0050308	Pitt_0050011	NYU_0051001	CMU_b_0050652
Trinity_0050251	UM_2_0050410	Pitt_0050016	UCLA_1_0051237	Pitt_0050007
Trinity_0050250	USM_0050531	Pitt_0050015	UCLA_1_0051235	Pitt_0050003
UCLA_1_0051219	Trinity_0050249	UCLA_1_0051231	UCLA_1_0051234	USM_0050532
UCLA_1_0051218	Trinity_0050242	USM_0050520	Pitt_0050057	UCLA_1_0051209
UCLA_1_0051215	Trinity_0050245	USM_0050525	Pitt_0050055	UCLA_1_0051206
UCLA_1_0051214	Trinity_0050246	NYU_0050987	Pitt_0050053	UCLA_1_0051205
USM_0050491	SBL_0051585	NYU_0050986	NYU_0050998	UCLA_1_0051201
USM_0050493	NYU_0051012	UM_2_0050402	Caltech_0051468	NYU_0050989
USM_0050492	UCLA_2_0051317	UM_2_0050406	UM_1_0050321	UM_1_0050285
UM_1_0050298	UCLA_1_0051223	UCLA_2_0051293	UM_1_0050320	Leuven_1_0050689

bioRxiv preprint doi: https://doi.org/10.1101/170381; this version posted July 9, 2019. The copyright holder for this preprint (which was not certified by peer review) is the author/funder, who has granted bioRxiv a license to display the preprint in perpetuity. It is made available under aCC-BY-NC-ND 4.0 International license.

Appendix B

The need for a trimmed estimator

In the Methods section, when describing the computation behind HiWeNet, we note that we remove 5% outliers from both tails of the thickness value distribution. The need to trim the distribution arises from the presence of several outlying values as can be seen from Fig. B1. There are large number of vertices with zero and very small values (which are zoomed-in in the right panel in Figure B) as well as few unnaturally large values (over 6mm), making it necessary to trim the patch-wise distributions to stabilize the distance estimates between a random pair of patch-wise histograms. We observe similar trends across all patch sizes (all values of *m*).

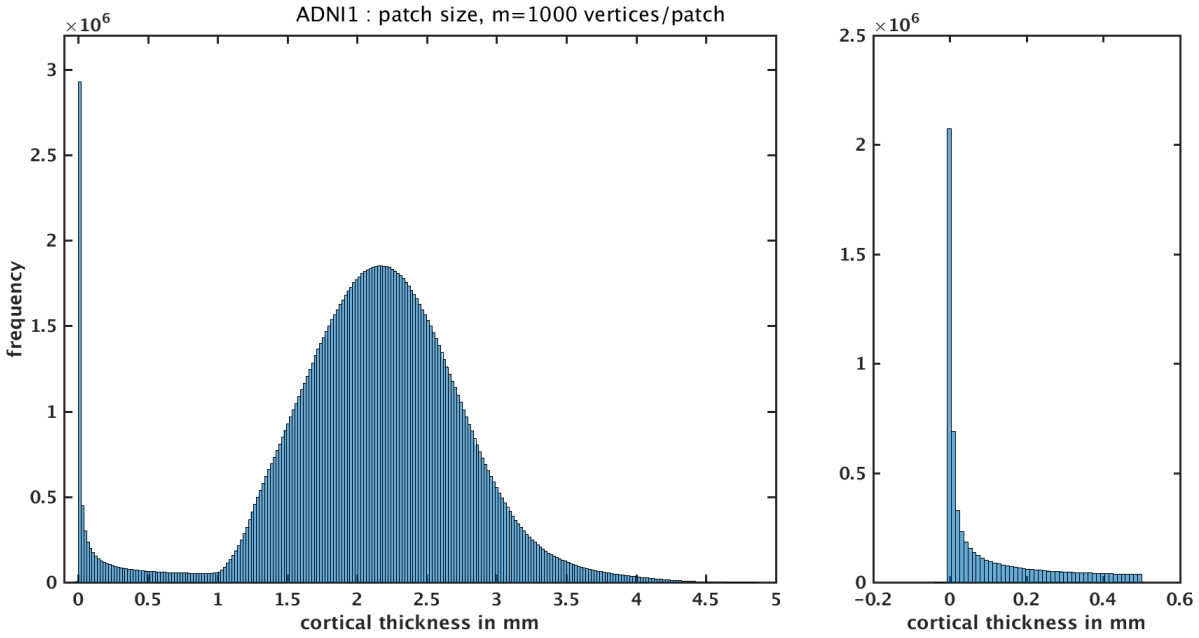

Figure B1: *the full distribution of thickness values from ADNI1 dataset using all the subjects (CN1, CN2, MCI and AD) included in this study. It is clear there are large number of vertices with zero and very small values, making it necessary to trim the patch-wise distributions to stabilize the distance estimates between a random pair of patch-wise histograms.*

Appendix C

To explore alternative representations for network-level features, we have extracted the following features: 1) compute a histogram for the distribution of thickness values from the entire cortex ('grand histogram'), and 2) for each patch, represent its value by the histogram distance between its own histogram and the grand mean histogram. Let's denote this method `relative_to_all` . This method results in a vector of length *n* only (number of patches for a given *m*) as opposed to fully-pairwise method adopted in this paper which results in *n*(n-1)/2* features. To understand their utility, we have evaluated their predictive performance for the 30 different feature sets based on `relative_to_all` edge weight. Their performance did not differ substantially from the fully-pairwise network-level counterparts - see the figure below. The median baseline performance (median of the 30 median AUCs each from 200 CV repetitions) is at AUC=0.89 in the CN1 vs. AD experiment (compared to AUC=0.87 for the fully-pairwise network features), at AUC= 0.77 (compared to AUC=0.75) for CN2 vs. MCIc and at AUC=0.56 (compared to AUC=0.6) for CN3 vs. AUT. Although the simpler relative_to_all method seems to perform just as well or slightly numerically better when the differences are pronounced (CN1 vs. AD and MCIc), it does slightly worse in the more challenging experiment (CN3 vs. AUT).

bioRxiv preprint doi: https://doi.org/10.1101/170381; this version posted July 9, 2019. The copyright holder for this preprint (which was not certified by peer review) is the author/funder, who has granted bioRxiv a license to display the preprint in perpetuity. It is made available under aCC-BY-NC-ND 4.0 International license.

This is consistent with our previous experience wherein fully-pairwise network-level features performed increasingly better as the predictive challenge increased with decreasing separability (Raamana et al. 2015). These results are now included in Appendix C.

We've also updated our open source *hiwenet* package to provide this feature, crediting this reviewer for the idea (anonymously).

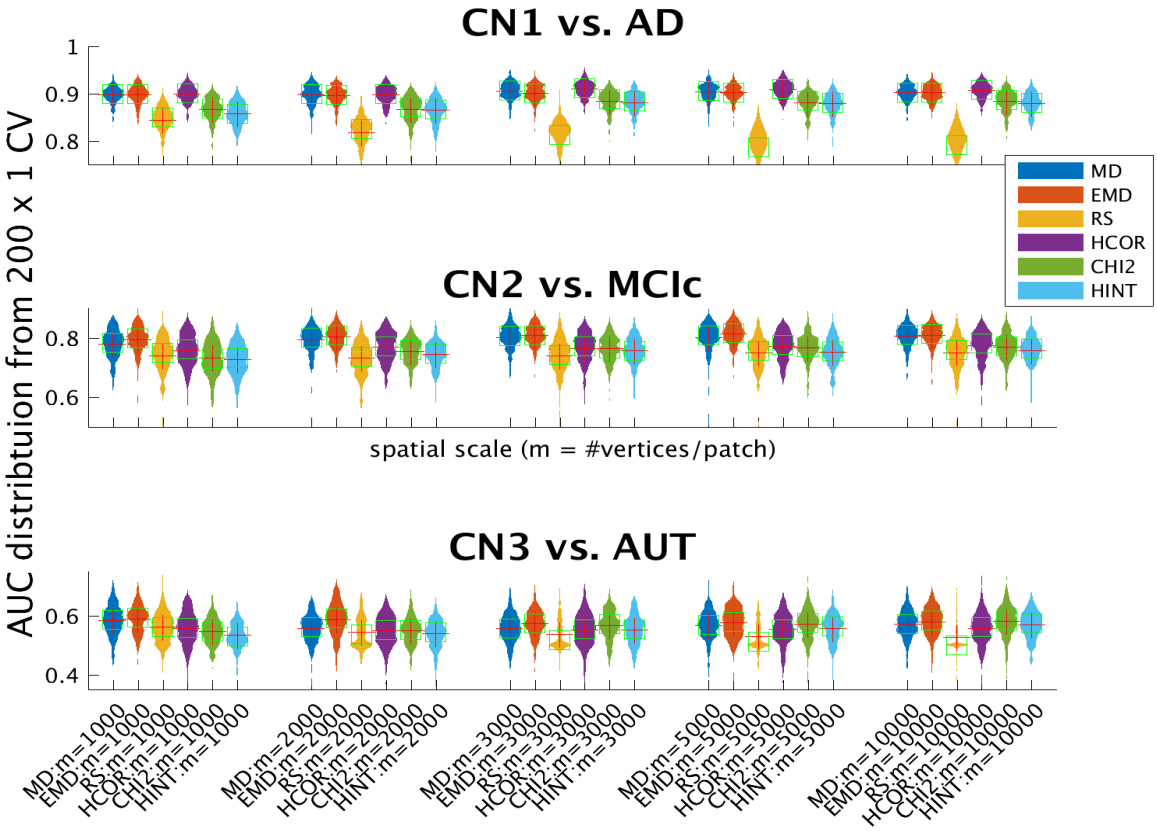

Appendix D

The sites represented per diagnostic group in the ABIDE dataset are shown in the table below:

Site	Controls	Autism
Pitt	21	10
NYU	17	19
Trinity	5	6
Leuven	16	10
KKI	3	3
USM	7	15
UM	12	12
MaxMun	1	1
SBL	5	1
UCLA	4	20
Caltech	1	1
Olin	4	0
Yale	3	0
SDSU	1	0
CMU	0	2